# The added value and potential of long-term radio occultation data for climatological wind field monitoring

Irena Nimac[1], Julia Danzer[1], Gottfried Kirchengast[1,2]

[1]Wegener Center for Climate and Global Change, University of Graz, Graz, 8010, Austria
5   [2]Institute of Physics, University of Graz, Graz, 8010, Austria

*Correspondence to*: Irena Nimac (irena.nimac@uni-graz.at) and Julia Danzer (julia.danzer@uni-graz.at)

**Abstract.** Global long-term stable 3D wind fields are a valuable information for climate-oriented analyses of the dynamics of the atmosphere. Their monitoring remains a challenging task, given shortcomings of available observations. One promising option for progress is the use of radio occultation (RO) satellite data, which enable deriving dynamics based on the
10   thermodynamics data. In this study we focus on three main goals, explored through European Re-Analysis ERA5 and RO datasets, using monthly-mean January and July data over 2007–2020. Our focus is on a $2.5° \times 2.5°$ spatial synoptic scale over the free-troposphere to the mid-stratosphere (i.e., 800 hPa – 10 hPa). First, by comparing ERA5-derived geostrophic and gradient wind speeds to the ERA5 original ones, we examine the regions of validity of the studied approximations at a given synoptic scale resolution. Second, to assess the possible added value of the RO-derived climatic winds in terms of their long-
15   term stability, we test the consistency with the corresponding ERA5-derived winds. Third, by comparing the RO climatic winds to the ERA5 original winds, we evaluate the potential benefit of RO as an additional dataset for wind analyses and climate monitoring. With this three-step analysis we decompose the total wind speed bias into the contributions from the approximation and the systematic difference between the RO and ERA5 datasets. We find that the geostrophic approximation is a valid method to estimate winds in the free troposphere, while the gradient wind approximation works better in the lower
20   stratosphere. Both approximations generally work well over the mentioned altitudes, within an accuracy of 2 m s$^{-1}$ for the latitudes 5°–82.5°. Exceptions are found in winter in the monsoonal area and above larger mountain ranges in the free troposphere, as well as above the northern polar regions in the mid-stratosphere. RO- and ERA5-derived geostrophic winds mostly showed good agreement (within 2 m s$^{-1}$). However, temporal change in the systematic difference higher than 0.5 m s$^{-1}$ per decade was found. This points to a possible impact of changes in the source of the assimilated data in ERA5. The overall
25   high accuracy of the monthly-mean wind fields, backed by the long-term stability and fine vertical resolution of the underlying RO data, highlights the added value and potential benefit of RO-derived climatic winds for climate monitoring and analyses.

# 1 Introduction

Wind field measurements have an important role in numerical weather prediction (NWP) and in atmospheric sciences for understanding climate dynamics and chemistry. As they serve as initial conditions in NWP models, their accuracy is of great importance. Besides, such data are also regularly assimilated in reanalysis systems, contributing to advances in climate science (Stoffelen et al., 2005; Eyre et al., 2020). Even though nowadays there is an increased portion of different techniques for measuring wind speeds, having accurate global 3D wind information is still a demanding task due to certain limitations of specific observation techniques (Stoffelen et al., 2005, 2020). While some techniques have generally good spatial coverage (e.g., meteorological stations, ships, buoys, scatterometer winds from satellite radars), they only provide wind information on single levels, lacking the vertical wind profile. On the other hand, techniques providing vertical profiles (e.g., wind profilers, radio-sounding data, pilot balloon data) have relatively coarse spatial coverage. Hence over larger parts in the southern hemisphere, such as oceans, both fine horizontal and vertical wind information is a problem (Stoffelen et al., 2005, 2020).

Altitude-resolving satellite data can help overcome these problems between profiling information and good global coverage. European Space Agency's (ESA) Earth Explorer mission Aeolus utilizes the active Doppler Wind Lidar method to measure wind from surface up to 30 km altitude (Stoffelen et al. 2005; Kanitz et al. 2019). The assimilation of this dataset resulted in improvement in NWP forecasts (Rennie et al., 2021; Žagar et al., 2021), as well as helped to better understand and analyse atmospheric dynamics such as Kelvin waves (Žagar et al., 2021) or gravity waves (Banyard et al., 2021). However, due to its quite short time period (launched in August 2018), these data are not suitable for climate change analyses. Another technique to derive vertical profiles is Global Navigation Satellite System (GNSS) radio occultation (RO), where the thermodynamic state of the atmosphere is obtained based on the transmitted GNSS radio signals refracted by the Earth's atmosphere (Kursinski et al., 1997; Steiner et al., 2011; Mannucci et al., 2020). The advantage of RO is its unique combination of global coverage, high vertical resolution, high accuracy, long-term stability, and multi-mission data consistency (e.g., Anthes, 2011; Foelsche et al., 2011; Angerer et al., 2017; Zeng et al., 2019; Steiner et al., 2020a). The RO data sets are assimilated into operational weather forecasts (e.g., Healy and Thépaut, 2006; Buontempo et al., 2008; Cardinali 2009) and long-term reanalyses (e.g., Hersbach et al., 2020; Kobayashi et al., 2015; Gelaro et al., 2017), and are used in climate analysis studies (e.g., Steiner et al., 2011, 2020b; Stocker et al., 2021).

While RO does not directly provide wind information, winds can be estimated from geopotential information using the conventional geostrophic and gradient wind approximations. The geostrophic approximation is a commonly used wind method in diagnostic studies. Although its utility in the mid-latitudes of the free troposphere was found to be good (e.g., Holton and Hakim, 2013; Boville 1987; Randel 1987), in the winter extratropical stratosphere significant overestimation of the polar jet stream (~10-20%) is found due to the neglect of local curvature effects (e.g., Boville 1987; Elson 1986; Randel 1987). Boville (1987) comments that the error in the meridional wind component is comparable to the error in the zonal wind component at all levels. To overcome this problem, one can use the gradient wind approximation which involves an additional centrifugal

60     term on top of the geostrophic balance. This method generally gives better results for stratospheric winds (e.g., Scherllin-Pirscher et al., 2014), however during intense wave activity, it produces large errors in high-latitude stratospheric regions (Elson 1986; Randel 1987).

Besides a seasonal and altitudinal dependence of the validity of the geostrophic and gradient wind approximation, another limitation is its breakdown towards the equatorial region as the Coriolis parameter approaches zero. Oberheide et al. (2002)

65     linearly interpolated geostrophic wind fields between ±10° latitude, Elson (1986) started with 4° N as the lowest latitude, Randel (1987) and Boville (1987) start at 10° N, while Scherllin-Pirscher et al. (2014) and Verkhoglyadova et al. (2014) left out the regions of ±15° and ±10°, respectively, from their wind estimation studies.

Even though the mentioned wind approximations are well demonstrated methods to derive dynamics from satellite information based on the mass (geopotential height) field (e.g., Oberheide et al., 2002; Scherllin-Pirscher et al., 2014, 2017;

70     Verkhoglyadova et al., 2014), their accuracy and validity for different latitudinal and altitudinal regions, as well as the regions of breaking-down, have not been thoroughly investigated. Several validation studies were made few decades ago using measurements such as rawinsonde (e.g., Wu and Jehn 1972) or climate models (e.g., Boville 1987; Randel 1987).

To our knowledge, there are no up-to-date studies dealing with a rigorous evaluation of the geostrophic and gradient wind approximations with a clear focus on climatological long-term wind field monitoring. This is especially important in regard to

75     recent improvements in both measurements and climate models in terms of temporal and spatial resolution as well as the parametrizations and processes included (Rummukainen, 2010). While Elson (1986) compared the estimated geostrophic wind with the one derived using higher-order approximations which accounted for horizontal wave flux convergence terms, Boville (1987) points out that such an approach does not give any information of how close the higher-order approximation is to the real wind. Hence, to test the quality of the used wind approximations, one needs to have a dataset which contains information

80     on both the pressure-geopotential height relation (thermodynamics) and the real wind (dynamics), such as climate model, reanalyses and operational analyses.

Hence in this study the main goal is to develop an RO-based climatic wind data product over the free troposphere (troposphere region above the planetary boundary layer - PBL) to the mid-stratosphere. The derived observations-based RO climatic wind fields have the potential to serve as a complementary climate-oriented dataset to reanalysis wind products. This is of specific

85     interest, since the uncertainties and errors in reanalyses are less well understood and more complex, due to changes in the assimilated data, as well as uncertainties arising from the weather forecast model used and the assimilation method (Parker 2016; Hoffman et al., 2017). On the other hand, RO data are long-term stable, essentially free from satellite-to-satellite bias and hence requiring no inter-satellite calibration, which leads to better known uncertainties and clear error characteristics (Steiner et al., 2020a).

90     The approach for the creation of RO climatic winds is three-fold. First, we test the approximation bias of the geostrophic and gradient-wind approximations. This serves as an information on the quality of this method for deriving monthly-mean winds

based on the thermodynamic mass fields (hereby called "climatic winds"). Therefore, we use ERA5 reanalysis data at the same synoptic-scale 2.5° × 2.5° spatial grid as RO. Second, we evaluate the difference between RO-derived winds and the ones estimated based on ERA5 data. Such a comparison of the systematic data bias helps reveal the added value of RO-derived

95 monthly-mean winds as an independent wind field record. Lastly, we evaluate the potential of RO-estimated winds in representing "original" ERA5 wind fields. To this end, we compare RO long-term monthly-mean winds with the original winds in ERA5. To test the robustness of estimated RO climatic winds, we perform an additional comparison with the ECMWF-IFS operational analyses for two selected test months, in a time frame when Aeolus data were assimilated.

The study builds upon and substantially advances a preliminary study by Nimac et al. (2023). The paper is structured as

100 follows: In Sect. 2 we describe the data and the method used in the study. The results are presented in Sect. 3, while Sect. 4 covers the discussion part. Conclusions and perspectives are finally given in Sect. 5.

## 2 Data and study method

In this analysis we used global monthly-mean ERA5 reanalysis (Hersbach et al., 2020) and multi-satellite RO OPSv5.6 data (Angerer at al., 2017; Steiner et al., 2020a) in the joint time period from 2007 to 2020. We analysed the global wind data at

105 2.5° latitude × 2.5° longitude grid in the altitude region from 800 hPa (~2 km) to 10 hPa (~32 km). We select 800 hPa as the lowest level in our analysis for the following reasons. First of all, this level is located above the PBL (e.g., Basha et al., 2019), a region where the studied wind approximations cannot capture such a complex dynamics. Second, in this altitude range RO data show the highest quality (Scherllin-Pirscher et al., 2017; Steiner et al., 2020a) with a core information strongly resulting just from RO observations. Towards higher and lower altitudes, the influence of background information increases in RO data

110 (OPSv5.6 uses ECMWF-IFS a s background). In the moist lower to middle troposphere region, background information of (re)analysis data supports the RO thermodynamic data retrieval from atmospheric refractivity (Scherllin-Pirscher et al., 2017; Li et al., 2019). Towards higher altitudes into the upper stratosphere, the impact of residual errors due to measurement noise and ionosphere starts to increase (e.g., Danzer et al., 2013, 2018; Liu et al., 2018), decreasing the accuracy of the RO-retrieved isobaric geopotential height data. Hence, we focus in our evaluation on the altitude range from the free troposphere (800 hPa

115 level) towards the mid-stratosphere (10 hPa level).

We chose January and July as two representative months for the winter and summer season. A further advantage of those two months is that the strongest wind speeds in jet stream regions are observed (e.g., Scherllin-Pirscher et al., 2014, 2017), reaffirming that these serve as an adequate test data for the goals of this study. For both months, we calculated the long-term monthly-mean wind speed fields over the 14-year period of 2007 to 2020.

120 We are aware that the ERA5 reanalysis also includes RO information, through its data assimilation process that ingested these and many other observation types, and hence depends also on RO data. However, all major state-of-the-art (re)analyses do assimilate RO data in our time range of interest since 2006 (start of the "U.S. COSMIC" and "European Metop" RO multi-

satellite era). Having an overall suitable and high-quality reference dataset, which does not assimilate RO data is hence essentially not feasible. For example, both JRA-55c and MERRA reanalyses do not assimilate RO data, while the recent

125    versions JRA-55 and MERRA-2 do so. However, there are also additional differences, such as JRA-55c does not assimilate any satellite data, which lowers the data quality in the upper troposphere and lower stratosphere drastically (Kawatani et al., 2020). Similarly, MERRA is based on an older model system, in quality inferior and not comparable to ERA5 or MERRA-2. With respect to our first goal of the analysis, which is to test the quality of the two approximations, the specific selection of the reanalysis dataset would hardly make a difference in the obtained results. However, the systematic difference might change

130    with a different reanalysis dataset. Considering the results from other studies that include also MERRA-2 and JRA-55 reanalyses (e.g., von Schuckmann et al., 2023, Sect. 3 therein, where atmospheric heat content change results built on changes in mass density fields), we can expect that the selection of the reanalysis dataset presumably has no major effect on the systematic difference for wind speeds derived from geopotential fields. We plan to perform a comparison with several reanalyses in our future research. In this study, as an additional evaluation of the robustness of the results, we utilize the

135    ECMWF-IFS analysis data for February and July 2020, a period when Aeolus data were assimilated.

## 2.1 ERA5 reanalysis data

As a state-of-the art reference dataset to test the validity of the geostrophic approximation, we used the European Re-Analysis 5th Version (ERA5) of the European Centre for Medium-Range Weather Forecasts (ECMWF). Even though ERA5 data is available on much finer $0.25° \times 0.25°$ spatial grid, in our study we retrieved ERA5 data on the $2.5°$ latitude $\times 2.5°$ longitude

140    grid to adjust it to the RO spatial grid. In the observed altitudinal range 800 hPa-10 hPa, ERA5 data were provided on 24 standard pressure levels with finer vertical resolution in the lower levels compared to the higher ones. For the selected monthly-mean data, we extracted eastward-wind and northward-wind components, for computing the original wind speeds, as well as isobaric geopotential height data (geopotential fields on pressure levels), for deriving the geostrophic winds and, on top of them, gradient winds. We term the ERA5 original wind speeds as $ERA_{orig}$, ERA5 geostrophic ones as $ERA_{geos}$, and ERA5

145    gradient winds as $ERA_{grad}$.

## 2.2 RO satellite data

The RO multi-satellite climatologies are derived from the satellite missions CHAMP (Wickert et al., 2001), C/NOFS (de la Beaujardiere et al., 2004), F3C (Anthes et al., 2008), GRACE (Beyerle et al., 2005; Wickert et al., 2005), MetOp (Luntama et al., 2008), and SAC-C (Hajj et al., 2004). Phase data were derived at UCAR/CDAAC (University Corporation for Atmospheric

150    Research/COSMIC Data Analysis and Archive Center), and further processed at the Wegener Center (WEGC) using the Occultation Processing System OPSv5.6 (Angerer et al., 2017; Steiner et al., 2020a). Based on the atmospheric bending of the

GNSS signals during the occultation sounding, it is possible to retrieve atmospheric refractivity profiles. From these, air density, temperature and pressure profiles as a function of altitude, or geopotential height, can be accurately derived based on the refractivity equation, the equation of state, and the downward integration of the hydrostatic equation (Scherllin-Pirscher et al., 2011a and b). In this way, geopotential height profiles as a function of pressure levels can be obtained with unique accuracy and form the basis for the wind field derivation (for a more detailed description see Scherllin-Pirscher et al., 2017).

The monthly-mean fields are calculated based on the daily RO climatological fields which are created by temporal and spatial weighting of RO atmospheric profiles. Temporal weighting is carried out within ±2 days, while spatial weighting is done within the constant radius of 600 km in order to maintain effective horizontal resolution. The profiles are weighted based on their distance from the centre location of a bin with a bivariate (latitude–longitude) Gaussian function, which has a peak at the centre of the bin and corresponding standard deviation of 150 km in latitudinal and 300 km in longitudinal direction, respectively. Details are given in the presentation by Ladstädter (2022). On average, the number of RO profiles is around 60 000 profiles per month. To derive the RO geostrophic wind speeds, we used monthly mean sampling error-corrected geopotential height data on isobaric surfaces, while gradient wind fields are further estimated based on the derived geostrophic wind. We term these RO-derived wind speeds as $RO_{geos}$ for geostrophic RO wind and $RO_{grad}$ for RO gradient wind.

### 2.3 Study method

We studied the regions of validity of the geostrophic and gradient wind approximation (first goal) as the difference of $ERA_{geos}$ and $ERA_{orig}$ wind fields and of $ERA_{grad}$ and $ERA_{orig}$ wind fields, respectively. This approach allows to study solely the bias resulting from the approximations. Further, we evaluated the differences of the RO-derived climatic winds from the reanalysis-derived ones (second goal) in terms of the $RO_{geos}$ vs. $ERA_{geos}$ difference (Fig. 1). By using this two-steps evaluation method, we first quantitatively test the adequacy and quality of the selected wind approximation methods based on the reanalysis data, while in the second step we estimate the systematic difference between RO and the reanalysis data for the wind derivation, which basically relates to a bias between the two datasets. The two-fold decomposition helps to attribute the individual contribution of each of the two biases (approximation and systematic) to the total difference between RO-derived wind field and ERA5 original winds.

For inspecting horizontal latitude-longitude maps, we concentrated on the four representative levels 200 hPa, 150 hPa, 50 hPa and 10 hPa, which represent the upper troposphere, tropopause, lower stratosphere and middle stratosphere regions, respectively. As a focus region, we examined latitudinal-altitudinal cross-sections of the respective wind speed differences averaged over 140°E–160°E longitudinal area. This longitudinal region is selected since the observed larger differences were mainly found there (i.e., roughly jet-stream core region). To assess the added value of RO data compared to ERA5 in terms of their temporal homogeneity and long-term stability, we analyse temporal differences in wind derived from two datasets.

To derive wind fields, one commonly starts with the equations of zonal and meridional momentum (Holton and Hakim 2013). However, due to the complexity of solving these non-linear partial differential equations, some assumptions and simplifications are useful to estimate approximate wind components. To derive them in line with the focus of this study from thermodynamic data (such as provided by RO) we first use the geostrophic approximation. In this approximation, most of the horizontal momentum equation terms are neglected, except for the Coriolis force term, which is balanced by the pressure gradient force. In the isobaric coordinate system, zonal ($u_{geos}$) and meridional ($v_{geos}$) geostrophic wind components are given by the relations (Holton and Hakim, 2013; Scherllin-Pirscher et al., 2014; Verkhoglyadova et al., 2014):

$$u_{geos} = \frac{-1}{f(\varphi)a}\frac{\partial \Phi}{\partial \varphi} \qquad (1)$$

$$v_{geos} = \frac{1}{f(\varphi)a\cos(\varphi)}\frac{\partial \Phi}{\partial \lambda} \qquad (2)$$

where $f(\varphi)$ is the local Coriolis parameter, $f(\varphi) = 2\Omega\sin\varphi$, with $\Omega = 7.2921\times10^{-5}$, $a$ is the Earth's radius, $\Phi$ denotes geopotential on isobaric levels, $\varphi$ is geographic latitude, and $\lambda$ longitude. Geopotential $\Phi$ is calculated as $\Phi = Z\,g_0$ where $Z$ is geopotential height and $g_0 = 9.80665$ m s$^{-2}$ the standard gravity constant. Hence, to derive geostrophic wind fields, we need geopotential height fields at pressure levels as information. As shown in Scherllin-Pirscher et al. (2017), alternatively the geostrophic wind could also be derived as the gradient vector of the Montgomery potential at potential temperature surfaces, but the results do not differ from the geopotential-based derivation used here.

Based on the estimated geostrophic wind speeds, the gradient wind approximation is used. In this approximation, the pressure gradient term is balanced not only by the Coriolis force but by the Coriolis and the centrifugal force together. The equations for zonal ($u_{grad}$) and meridional ($v_{grad}$) gradient wind components are hence functions involving the geostrophic wind components as their backbone, calculated as (Holton and Hakim, 2013; Scherllin-Pirscher et al., 2014):

$$u_{grad} = F(u_{geos}, \varphi) = \frac{-f(\varphi) \pm \sqrt{f^2(\varphi) + 4f(\varphi)u_{geos}\tan(\varphi)/a}}{2\tan(\varphi)/a} \qquad (3)$$

$$v_{grad} = F(v_{geos}, u_{grad}, \varphi) = \frac{v_{geos}f(\varphi)}{f(\varphi) + u_{grad}\tan(\varphi)/a} \qquad (4)$$

Here, the +/- sign refers to Northern (+) resp. Southern Hemisphere (–). The total wind speed is calculated as a squared root of the sum of the squared zonal and meridional wind components, and we term this $V_{orig}$ for the original wind, $V_{geos}$ for the geostrophic wind and $V_{grad}$ for the gradient wind.

This procedure was applied to both ERA5 and RO geopotential fields to estimate corresponding geostrophic winds and gradient winds. To assess the added value of the gradient wind approximation on top of the geostrophic approximation, we estimate the gradient wind delta-difference field $\Delta V$ defined as:

$$\Delta V = |Bias_{geos}| - |Bias_{grad}| = |V_{geos} - V_{orig}| - |V_{grad} - V_{orig}|, \qquad (5)$$

$$\Delta V > 0 \rightarrow |Bias_{grad}| < |Bias_{geos}|,$$

$$\Delta V < 0 \rightarrow \left| Bias_{geos} \right| < \left| Bias_{grad} \right|.$$

In using this convenient absolute delta-difference metric for inspecting the additional bias reduction or bias increase by the gradient wind approximation vs. the geostrophic approximation, the regions where both approximations give similar values will be suppressed (delta-difference near zero), while areas with larger delta-difference will stand out. Positive delta-difference
215 values indicate better estimation of the original wind by the gradient wind approximation, while negative delta-difference values represent the opposite – better representation of the original wind by the geostrophic approximation.

Since deriving geostrophic wind fields is based on the horizontal derivatives of geopotential height, it is desirable for the geopotential height field to be smooth. As the ERA5 geopotential field is derived by numerical integration, it is smoother compared to the observation-based RO geopotential field. Hence, we smoothed the $2.5° \times 2.5°$ RO geopotential fields using a
220 5-point Gaussian filter in longitudinal and latitudinal direction. In the latitudinal direction, the last two latitude circle grid lines were excluded from the analysis, since they are needed as filter margin. Additionally, one more grid line ($85°$) was discarded after calculating the derivative according to Eq. (1). The final latitudinal range used for the RO-derived fields is $\pm82.5°$. Related to this, due to the lower number of soundings over the polar caps (as well as the complexity of calculations over polar regions), it is justified to exclude these few polar latitude circles from the analysis in both RO and ERA5 wind fields.

225 Such filtering smoothes not only the noise component, but part of the signal too. Hence the spatial resolution of the field decreases (Vishwakarma et al., 2018). The amplitude of the damped signal depends on the selected type of filter. For a Gaussian filter the resulting resolution of the fields gets coarser by a factor of two, compared to the smoothing radius (Devarju, 2015). Overall, it is clear that there are differences in the spatio-temporal representation of ERA5 and RO data. Regarding the temporal component, we can assume that temporal weighting applied to the daily RO profiles does not strongly influence the monthly-
230 mean value. On the other hand, ERA5 (and ECMWF-IFS model) winds are also filtered by spatial and temporal diffusion operators (Hersbach et al., 2020). In summary, these post-processing methods affect the physical spatial resolution of the field. To estimate the effective physical resolution of the resulting climatic field is hence not an easy task (e.g., Vishwakarma et al., 2018). We plan to investigate this aspect more thoroughly in our future research by testing various filtering options and inspecting their influence on wind fields over mountainous regions, where fine horizontal structures are usually observed.

235 As the Coriolis parameter $f(\varphi)$ approaches zero near the equator, the approximations are not valid in those areas. A separate wind analysis based on the thermal wind balance was done by Danzer et al. (2024) for the equatorial region. Still, as in our data grids the lowest latitude bin grid lines are at $\pm1.25°$ latitude, it was possible to calculate winds for all climatological bins, though values close to the equator lose physical meaning. This way we determined the region of approximation break-down by comparing the approximation bias to some commonly used accuracy requirement values.

240 We used the monthly-mean geopotential data at isobaric levels for the January and July months in the period 2007–2020 to derive the geostrophic wind components using equations (1) and (2), and gradient wind by equations (3) and (4), and subsequently computed the speed as the magnitude of the corresponding wind vector. The wind speeds for ERA$_{orig}$, ERA$_{geos}$,

RO$_{geos}$, ERA$_{grad}$ and RO$_{grad}$ were then used to perform our evaluations according to Fig. 1. All calculations, statistical analysis and visualization were performed using Python programming language and mainly its packages *numpy, xarray, pymannkendall* and *matplotlib*.

To put the results into context with reasonable wind accuracy requirements (e.g., Stoffelen et al., 2020), we used absolute requirement values for domains with small wind speeds, while for large wind speeds relative requirement values appear a more appropriate choice. We chose a difference of $\pm 2$ m s$^{-1}$ or a relative difference of $\pm 5$ % as requirements, which are values consistent with the wind observation accuracy target requirements specified by the World Meteorological Organization (WMO) for various applications, including NWP and climate (Stoffelen et al., 2020; WMO-OSCAR, 2022; Table 1). Simple linear regression was used to test the long-term temporal stability of the derived wind speed fields. We estimated the decadal trend rate in difference between RO$_{geos}$ and ERA$_{geos}$ and evaluated this against the WMO-GCOS (2016) wind measurement stability target requirement of $\pm 0.5$ m s$^{-1}$ per decade (see also Table 1).
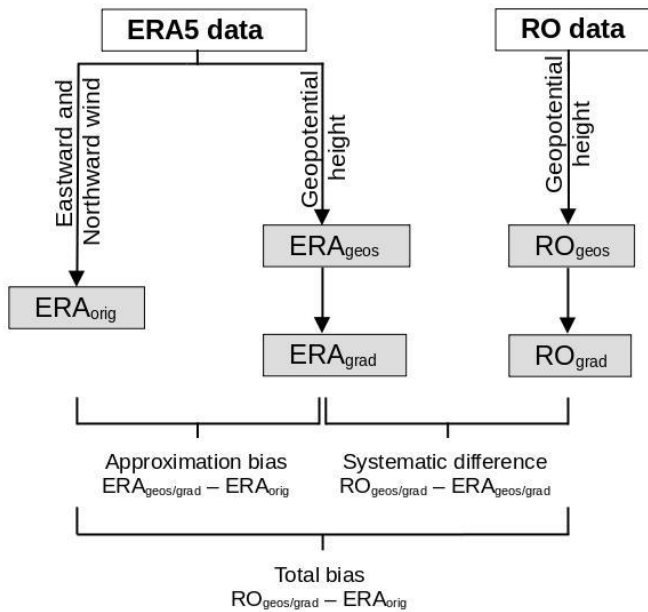
**Figure 1:** Schematic diagram of the three-steps evaluation method. The original ERA5 (ERA$_{orig}$) wind speed is calculated based on the northward and eastward wind components. In the first step, geostrophic ERA5 (ERA$_{geos}$) and geostrophic RO (RO$_{geos}$) winds are estimated from the corresponding geopotential height data. In the second step, ERA5 gradient (ERA$_{grad}$) and RO gradient (RO$_{grad}$) winds are calculated using previously derived ERA$_{geos}$ and RO$_{geos}$, respectively. Approximation bias

is computed as a difference between the estimated $ERA_{geos}$ and $ERA_{grad}$ relative to $ERA_{orig}$, while the datasets' systematic difference is computed as the difference in corresponding wind fields, $ERA_{geos}$ and $RO_{geos}$ or $ERA_{grad}$ and $RO_{grad}$, respectively. Total bias is computed as the difference between estimated RO winds and $ERA_{orig}$.

**Table 1:** Selected absolute and relative wind speed accuracy requirements used in the study, informed by WMO-GCOS (2016).

| Accuracy Specifications | Absolute | Relative |
|---|---|---|
| Evaluation of wind approximations | $\pm 2$ m s$^{-1}$ | $\pm 5$ % |
| Temporal stability check | $\pm 0.5$ m s$^{-1}$ per decade | - |

## 3 Results

### 3.1 Approximation bias – $ERA_{geos}$ and $ERA_{grad}$ vs. $ERA_{orig}$

To test the strengths and weaknesses of the geostrophic and gradient wind approximations, we compare estimated $ERA_{geos}$ and $ERA_{grad}$ to the original $ERA_{orig}$ winds for January (Fig. 2) and July (Fig. 3). We show the ageostrophic contribution as a reference bias field, while for gradient wind we present delta-differences calculated based on the equation (5). This delta-difference approach allows us to show only regions where gradient wind approximation estimates original wind notably better (i.e., positive delta-difference values) or notably worse (i.e., negative delta-difference values) compared to the geostrophic balance. Hence, where the delta-difference is small, the approximations give relatively similar wind estimations.

For both approximations some same deviations from the original wind are observed in the regions where the centrifugal term does not contribute much (i.e., in equatorial and tropical regions). At two lower selected levels and in both seasons, the largest amplitude of the differences is found around the equator from -5° to 5° latitude, as a result of the Coriolis parameter approaching zero. These differences are clearly larger than the selected accuracy threshold of 2 m s$^{-1}$, indicating the region of approximation break down. At lower levels, larger underestimation of original wind is observed in monsoonal regions over Indonesia in January and tropical Indian Ocean in July (Fig. 2c, Fig. 3c). Larger positive biases (up to 6 m s$^{-1}$) are observed in the sub-tropical jet stream on the winter hemisphere. At the lowest 200 hPa level, a glimpse of stationary waves is noticeable as a dipole structure above western part of the Northern America, as well as a dipole over SW Asia (Fig. 2a).

The largest differences between the geostrophic and the gradient wind approximations are present at the lowest 200 hPa (Fig. 2a-b, Fig. 3a-b) and at the highest 10 hPa (Fig. 2g-h, Fig. 3g-h) observed levels. The geostrophic balance describes the original wind better at the lower levels, especially over the Pacific Ocean in the regions of the sub-tropical jet stream core where gradient wind approximation underestimations original wind (~ ±30° lat) (Fig. 2a and Fig. 3a). On the other hand, the gradient

wind performs better in the lower and mid-stratosphere regions, specifically for depicting the polar stratospheric jet-stream (~ ±60° lat) (Fig. 2h and Fig. 3h). The gradient wind balance works better for July stratospheric winds, unlike in January when it

290    significantly underestimates wind in the northernmost polar regions.
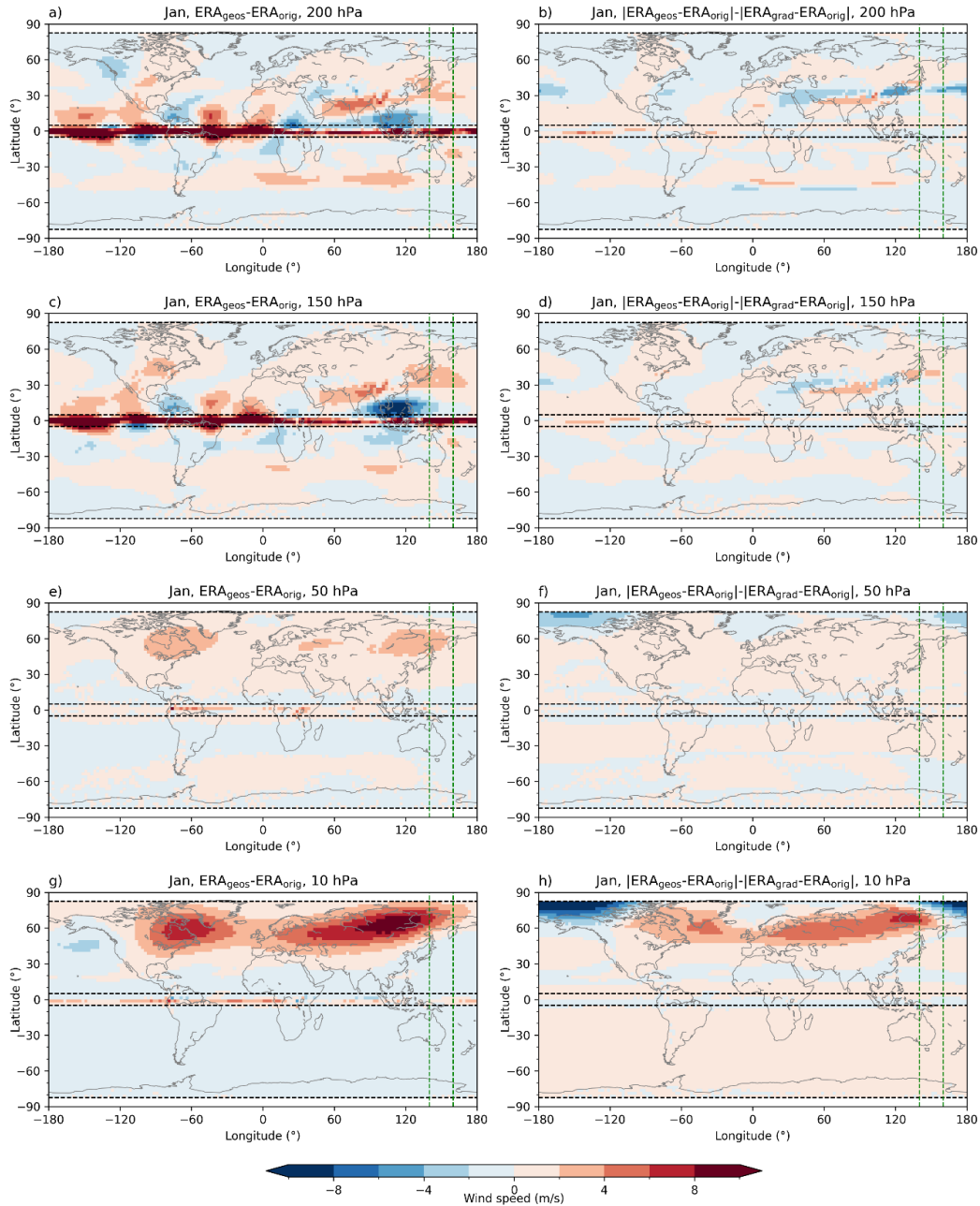
**Figure 2:** Long-term (2007–2020) mean approximation bias. Wind speed differences (m s$^{-1}$) between the geostrophic ERA5 (ERA$_{geos}$) and the original ERA5 (ERA$_{orig}$) wind (left column), and the gradient wind (ERA$_{grad}$) delta-difference calculated using equation (5) (right column), at the 200 hPa (first row), 150 hPa (second row), 50 hPa (third row) and 10 hPa (last row)

level for January. Dashed green vertical lines denote the 140°–160° E area for which vertical cross-section is given. Dashed black horizontal lines delineate the ±5° latitude band around the equator and ±82.5° regions toward poles.
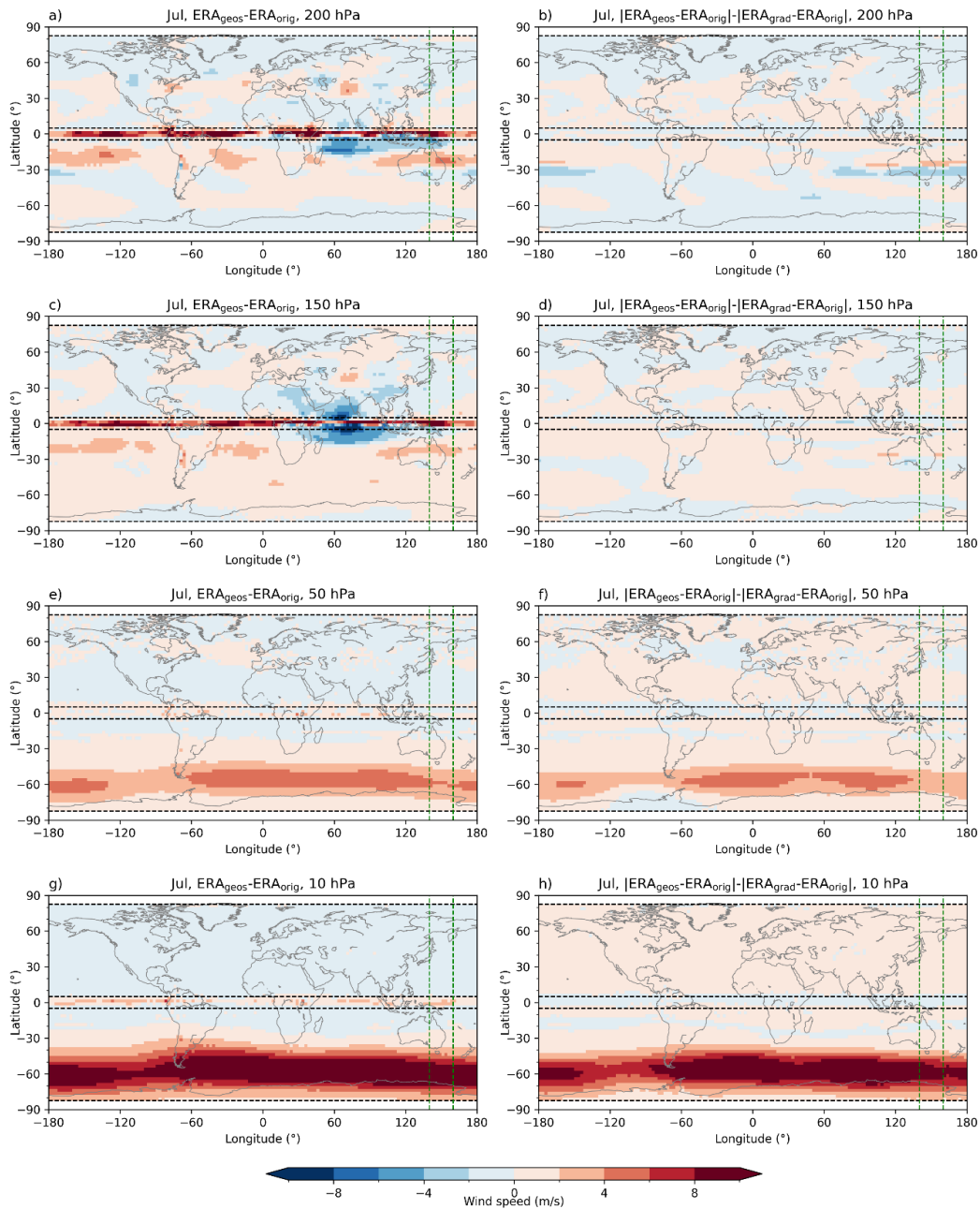
**Figure 3:** The same as in Fig. 2 but for July.

To better understand the altitudinal-latitudinal behaviour of both approximation biases, we examine its latitudinal vertical cross-section averaged over the region 140°–160° E (Fig. 4). This longitudinal region is selected because both larger deviations from sub-tropical and polar jet-stream are found here (i.e., region of strengths and weaknesses of geostrophic and gradient wind approximation). In both seasons, both approximations are not valid in the equatorial region between ±5° latitude. Generally, the geostrophic approximation is better in describing the dynamics of the sub-tropical jet stream, while the gradient wind approximation works better at higher levels since the delta-difference is there positive, especially during SH winter. An underestimation of the NH stratospheric polar jet stream by the gradient wind approximation is noticeable through negative delta-difference values in the high-latitude regions (Fig. 4b). Except for the mentioned larger deviations in describing sub-tropical or polar jet-stream, wind speed differences are well within the accuracy requirement of 2 m s$^{-1}$.
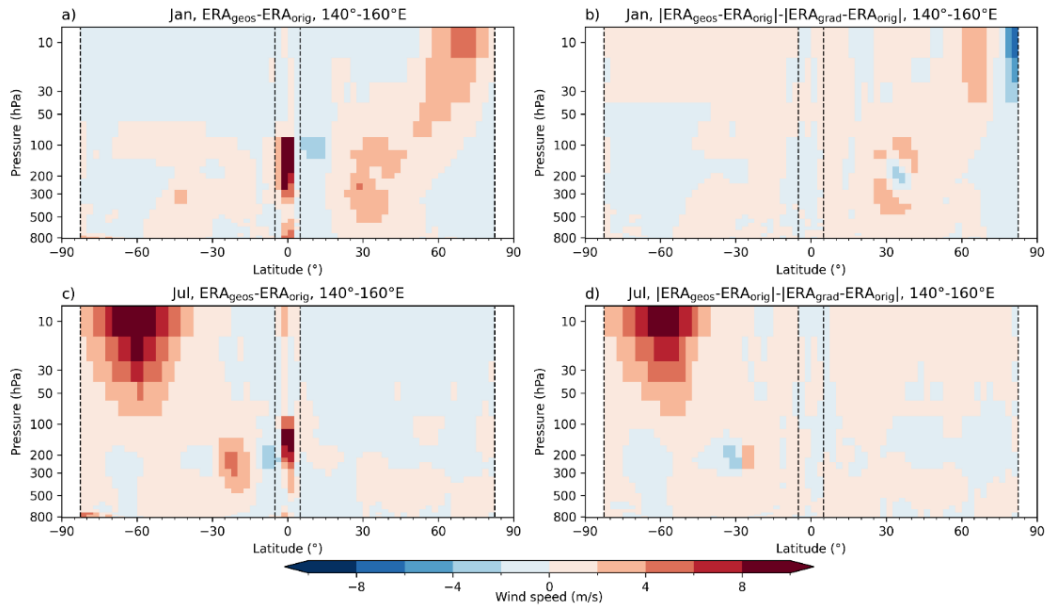
**Figure 4:** Long-term (2007–2020) mean vertical cross-section of the approximation bias. Wind speed differences (m s$^{-1}$) between the geostrophic ERA5 (ERA$_{geos}$) and the original ERA5 (ERA$_{orig}$) wind (left column) and the gradient wind (ERA$_{grad}$) delta-difference calculated using equation (5) (right column), averaged over the 140°–160° E area for January (top) and July (bottom). Dashed black vertical lines delineate the ±5° latitude band around the equator and ±82.5° regions toward poles.

## 3.2 Systematic difference – RO$_{geos/grad}$ vs. ERA$_{geos/grad}$

In line with the second study goal, we tested how well RO-derived and estimated ERA5 wind fields agree, applying for both data products the same approximation. Building upon the results from Sect. 3.1, the equatorial band within ±5° is excluded from further inspections. We focus on understanding the consistency between RO and ERA5 estimated wind speed in those (still) nearly global domains, where the approximations are found to perform well. Since this systematic difference between the two datasets (RO vs. ERA5) is equal for geostrophic and gradient wind, for convenience we show the results only for geostrophic wind.

An inspection of the differences in horizontal maps at four selected levels reveals that the overall wind patterns are well represented by the RO wind data (Fig. 5). Generally, the differences are larger over the winter hemisphere, especially in the region of subtropical jet stream at 200 hPa where RO$_{geos}$ over-/underestimates ERA$_{geos}$ around ±20°/30° latitude, respectively (Fig. 5a, b). Such pattern might indicate that, based on the geopotential data, the position of the jet stream is slightly moved further equator-ward in RO data compared to the ERA5 dataset. This difference is still present at 150 hPa level, but with lower amplitudes (Fig. 5c, d). At 50 hPa, differences are well within ±2 m s$^{-1}$ (Fig. 5e, f). In both seasons, at the highest level of 10 hPa differences up to 4 m s$^{-1}$ are found in the tropical region (Fig. 5g-h).

Investigating the latitudinal cross-section confirms that the observed larger differences (up to around 6 m s$^{-1}$) in the winter hemisphere correspond to the locations of the sub-tropical jet-stream (Fig. 6). A maximum January amplitude, showing a positive difference at ~300 hPa and a negative at ~200 hPa, might also point to a somewhat lower location of the jet-stream core in RO data compared to the ERA5 data (Fig. 6a). In July, such a difference in the location of the jet-stream core between the two datasets is not noticeable (Fig. 6b).
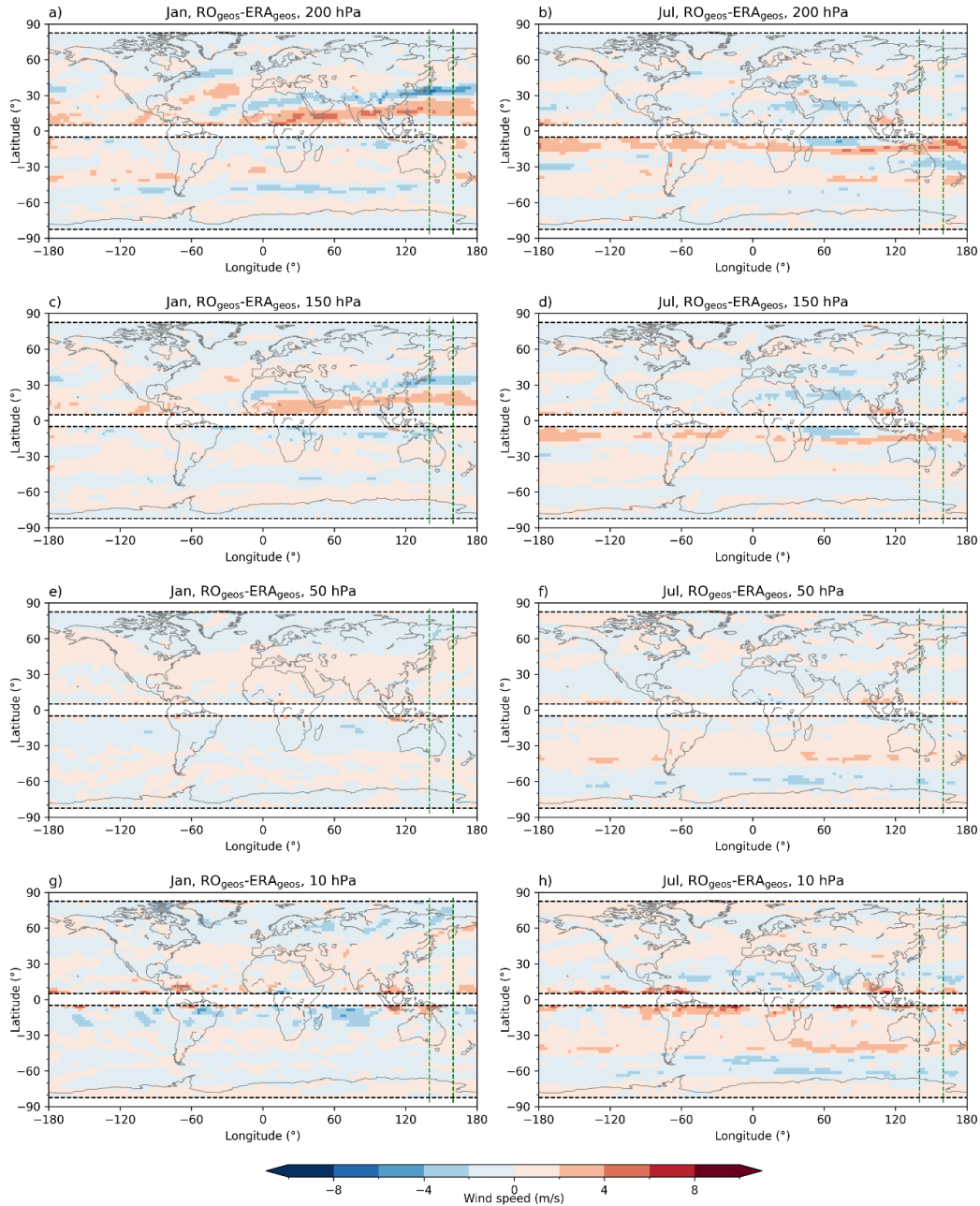
**Figure 5:** Long-term (2007–2020) mean systematic difference between RO and ERA5. Wind speed differences (m s$^{-1}$) between the geostrophic RO (RO$_{geos}$) and the geostrophic ERA5 (ERA$_{geos}$) wind, at 200 hPa (first row), 150 hPa (second row), 50 hPa (third row) and 10 hPa (last row), for January (left column) and July (right column). Dashed green vertical lines denote the

140°–160° E area for which vertical cross-section is given. Dashed black vertical lines delineate the ±5° latitude band around the equator and ±82.5° regions toward poles.
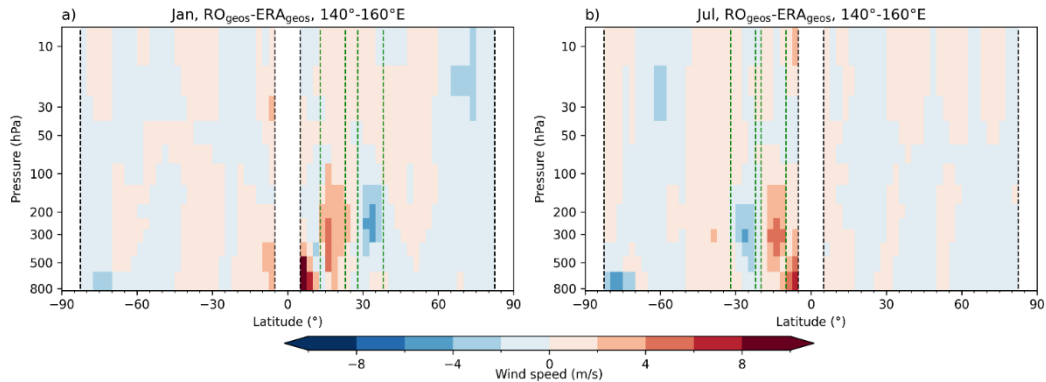
345

**Figure 6:** Long-term (2007–2020) mean vertical cross-section of the systematic difference between RO and ERA5. Wind speed differences (m s$^{-1}$) between the geostrophic RO (RO$_{geos}$) and the geostrophic ERA5 (ERA$_{geos}$) wind, averaged over the 140°–160° E area for January (left) and July (right). Dashed green vertical lines denote latitudinal belts used in the further analysis of long-term temporal consistency of the datasets. Dashed black vertical lines delineate the ±5° latitude band around
350 the equator and ±82.5° regions toward poles.

To better understand these systematic differences, we investigate its latitudinal and altitudinal temporal variations over the longitude sector 140°–160° E. This longitude sector was selected, because the subtropical jet stream seems to leave a quite distinct feature over the western Pacific; differences of up to ±6 m s$^{-1}$ (i.e., up to exceeding the Table 1 threshold requirements)
355 are seen in this sector in the winter hemisphere (see Fig. 5a, b).

A 2007–2020 temporal analysis (Fig. 7) reveals that this pattern is systematic, with belts of positive and negative differences within 10° to 40° latitude in the winter hemisphere (Fig. 7a, c). We therefore further define equally wide latitudinal belts that encompass the discussed over- and underestimations to estimate the value of its temporal change. In January, we define the regions of RO-derived wind over-/underestimation within the latitudinal belt 13°–23° N/28°–38° N, while for July it is 10°–
360 20° S/22°–32° S, respectively. The time-series analysis revealed that both, the positive and negative differences between the two datasets, decrease with time (Fig. 7b, d). Exceedance of the WMO-GCOS target requirement (Tab. 1) for long-term stability within ±0.5 m s$^{-1}$ per decade, taken as a consistency benchmark, is at 200 hPa level detected in both seasons for negative differences and in July for positive difference as well (Fig. 7b, d). However, when calculated at other levels, e.g., 300 hPa or 250 hPa, the bias in the region of RO-wind overestimation is in January below ±0.5 m s$^{-1}$ threshold (Tab. 2).
365 The explanation to this result is shown in the Fig. 8. Besides the temporal change in its amplitude, we also find an altitudinal shift in the systematic difference. This is more expressed for belts where RO$_{geos}$ overestimates ERA$_{geos}$ wind. From that, we

can conclude that an analysis of changes in the jet-stream core position based on ERA5 and RO data can give somewhat different results. Such detected temporal and altitudinal differences in the systematic bias might correspond to major observing system changes in the ERA5 data assimilation (Hersbach et al., 2020; Fig. 3 and 4 therein).

370
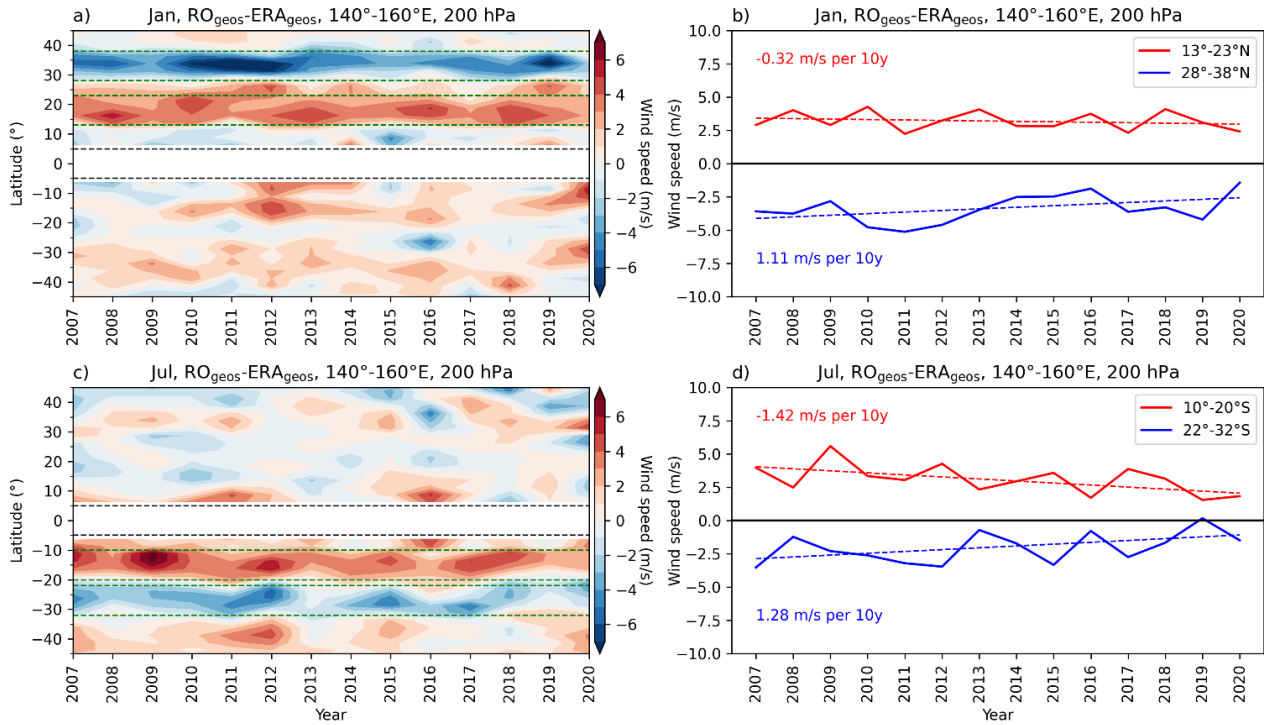
**Figure 7:** Latitudinal temporal distribution of the systematic difference between RO and ERA5. Wind speed difference (m s^{-1}) between the geostrophic RO (RO$_{geos}$) and the geostrophic ERA5 (ERA$_{geos}$) wind, averaged over the 140°–160° E area at 200 hPa (left column), for January (top) and July (bottom). Dashed green horizontal lines denote 10° latitudinal belts 13°–23° N and 28°–38° N in January, and 10°–20° S and 22°–32°S in July, for which the temporal trend analysis is made (right column and Table 2). Black dashed horizontal lines delineate the ±5° equator band.
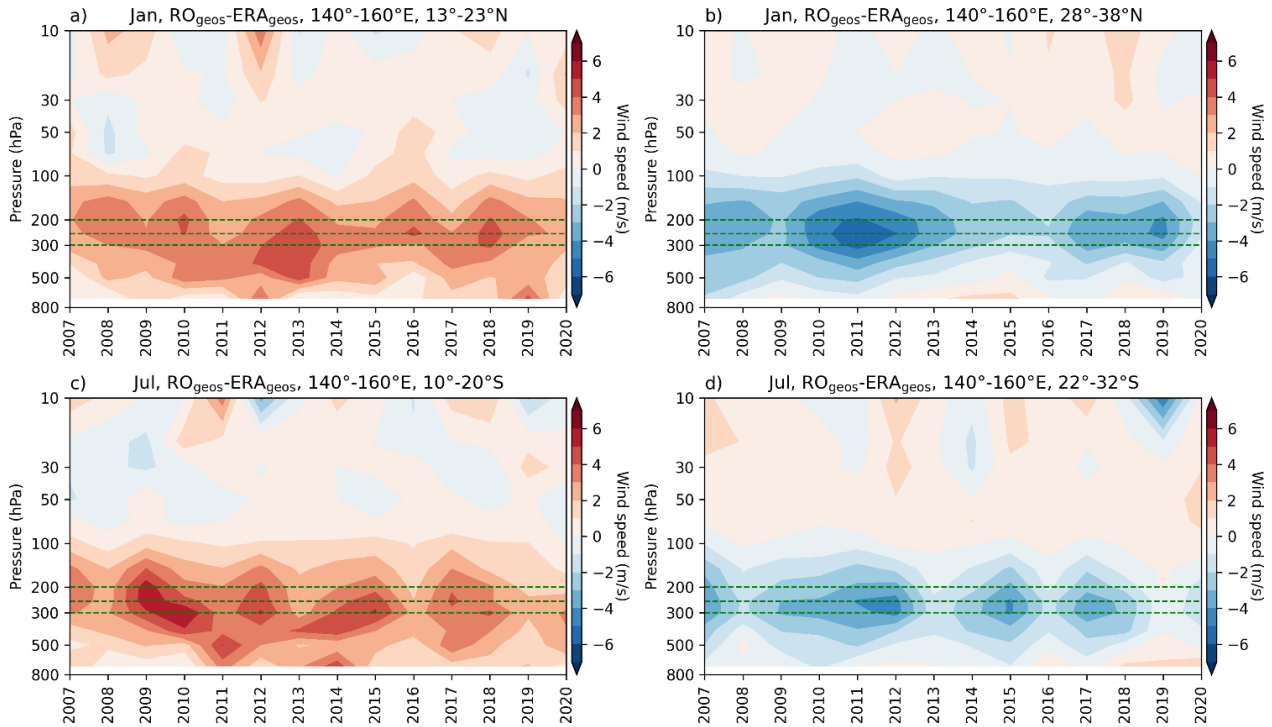
**Figure 8:** Altitudinal temporal distribution of the systematic difference between RO and ERA5. Wind speed difference (m s⁻¹) between the geostrophic RO (RO$_{geos}$) and the geostrophic ERA5 (ERA$_{geos}$) wind, averaged over the 140°–160° E area for a) 13°–23° N and b) 28°–38° N in January, and c) 10°–20° S and d) 22°–32° S in July. Dashed green lines denote 200 hPa, 250 hPa and 300 hPa levels for which the decadal trend values are given in the Table 2.

**Table 2.** Decadal trend values (m s-1 per decade) in the systematic difference between the geostrophic RO and the geostrophic ERA5 wind speeds, averaged over 140°–160° E longitudinal area and latitudinal regions 13-23° N and 28°-38° N in January, and 10°-20° S and 22°-32° S in July, at 200 hPa, 250 hPa and 300 hPa levels. Systematic-difference trend rates larger than the WMO-GCOS (2016) long-term stability requirement of ±0.5 m s$^{-1}$ per decade (Table 1) are bold-faced.

| | | Trend rate (m/s per decade) | | |
| --- | --- | --- | --- | --- |
| | | 200 hPa | 250 hPa | 300 hPa |
| January | 13-23° N | -0.32 | 0.21 | -0.20 |
| | 28-38° N | **1.11** | **1.16** | **1.35** |
| July | 10-20° S | **-1.42** | **-1.15** | **-0.65** |
| | 22-32° S | **1.28** | **1.29** | **1.21** |

390

### 3.3 Total bias – RO$_{geos/grad}$ vs. ERA$_{orig}$

395    In the final step, we show the total wind speed bias, i.e., how well is the original ERA5 wind field estimated by RO-derived winds. Here, we evaluate the total wind speed bias in regard to WMO-related requirements (Tab. 1).

At the lowest observed level (200 hPa), in both seasons RO$_{geos}$ gives better estimates of ERA$_{orig}$ compared to RO$_{grad}$. For RO$_{geos}$ these differences are generally below 2 m s$^{-1}$, except from the slight overestimation (~3 m s$^{-1}$) at ~15° winter hemisphere latitude (Fig. 9a-b). Generally good agreement of RO$_{geos}$ and ERA$_{orig}$ is also observed at 150 hPa level, with a bit lower

400    overestimation at ~15° winter hemisphere latitude (Fig. 9c-d). At 50 hPa level, both approximations give January wind estimations with bias bellow 2 m s$^{-1}$, while in July RO$_{geos}$ overestimates ERA$_{orig}$ wind at ~60° S for around 4 m s$^{-1}$ (Fig. 9e-f). At the highest selected level (10 hPa), RO$_{geos}$ overestimates ERA$_{orig}$ for around 4 m s$^{-1}$ at 60° N, while RO$_{grad}$ underestimates it for ~4 m s$^{-1}$ in high-latitude polar regions (Fig. 9g). On the other hand, in July, RO$_{geos}$ overestimation over southern hemisphere is larger than 10 m s$^{-1}$, while RO$_{grad}$ gives estimates with accuracy within 2 m s$^{-1}$ (Fig. 9h).

405    Hence, in the last step we show horizontal fields of the total bias between RO-derived and original ERA5 wind at selected levels, where we show RO$_{geos}$ winds for the two lower levels, and RO$_{grad}$ wind in the upper two levels.

Based on the results shown in the previous sections, it is clear that the total bias in the sub-tropical jet stream is a result of the systematic difference and the approximation bias (Fig. 10a-b). On the other hand, a larger underestimation of winds by RO$_{geos}$ in the monsoonal region, as well as dipole structures related to stationary waves are mainly a result of the inability of the

410    geostrophic approximation to capture such a circulation (Fig. 10c-d). Similar patterns can be seen in the Figure A1a- b, where a comparison between RO geostrophic wind speeds and ECMWF-IFS analysis wind speeds at 200 hPa for February and July 2020 is shown as a complementary information. However, as to be expected, the Fig. A1 differences exhibit more details and a larger spatial variability compared to Fig. 10, where variability is lower due to the temporal averaging.

In the upper levels, the total bias is mainly the result of the applied approximation (Fig. 10e-h). The exception is the tropical

415    region where lower RO data quality contributes to somewhat larger bias. The NH high-latitude RO$_{grad}$ wind underestimation in January is caused by neglecting the horizontal advection terms, which are important during condition when strong wave activity and polar night jet interact. Again, the robustness of the results is supported by a further complementary comparison with two test months of ECMWF-IFS analysis data (Appendix Fig. A1c-d). Similar patterns are observed, with stronger expressed noise-like differences near the equator.

420
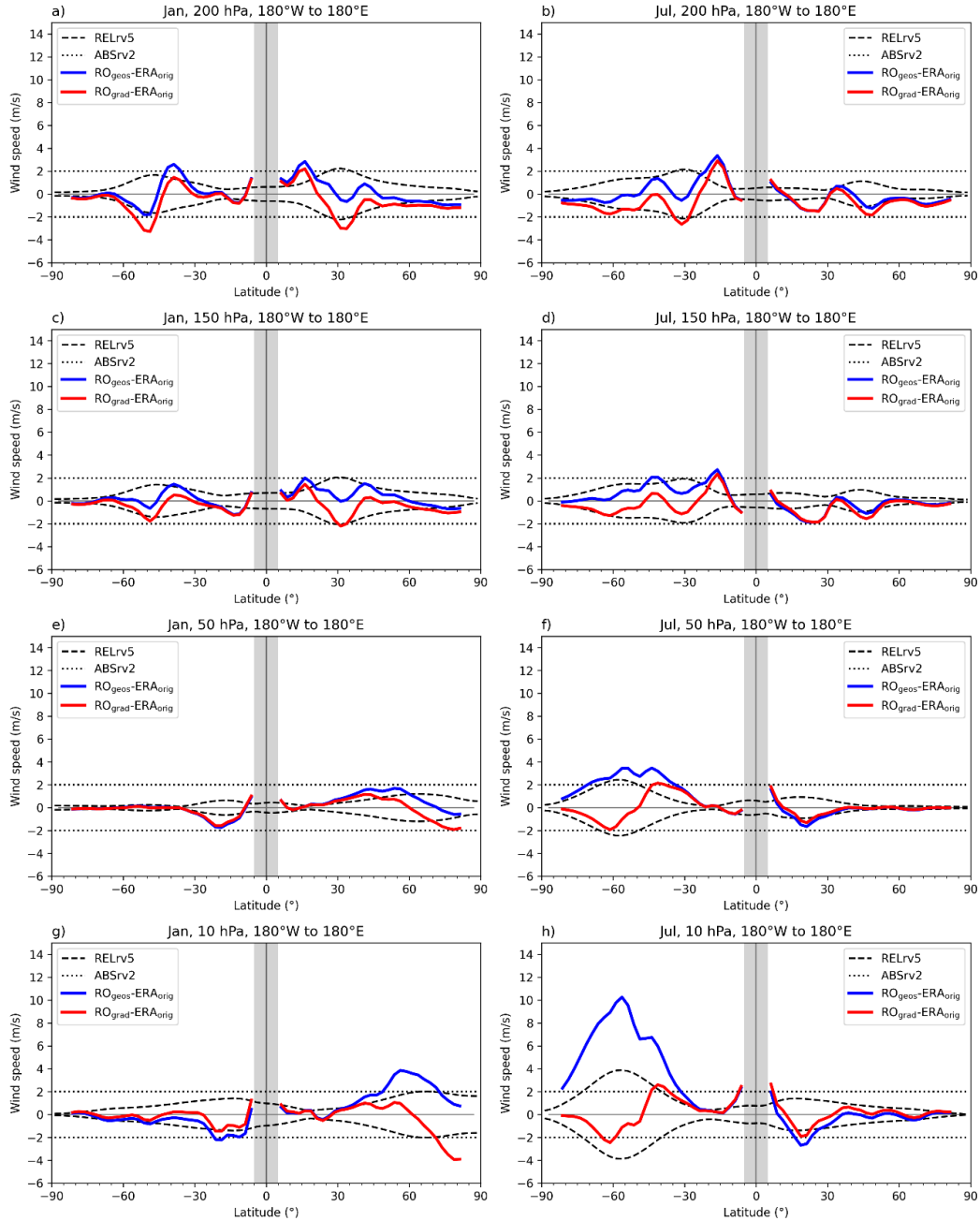
**Figure 9:** Latitudinal distribution of the total bias. Wind speed difference (m s$^{-1}$) between the geostrophic RO (RO$_{geos}$) and the original ERA5 (ERA$_{orig}$) wind (blue line) and between the gradient RO (RO$_{grad}$) and the original ERA5 (ERA$_{orig}$) wind (red line), at the 200 hPa (first row), 150 hPa (second row), 50 hPa (third row) and 10 hPa (last row) level, for January (left column)

and July (right column). WMO-based accuracy requirement values are indicated in absolute terms at values of 2 m s$^{-1}$ (ABSrv2, dotted black line) and in relative terms at 5 %, with reference to the original ERA5 wind speed (RELrv5, dashed black line).
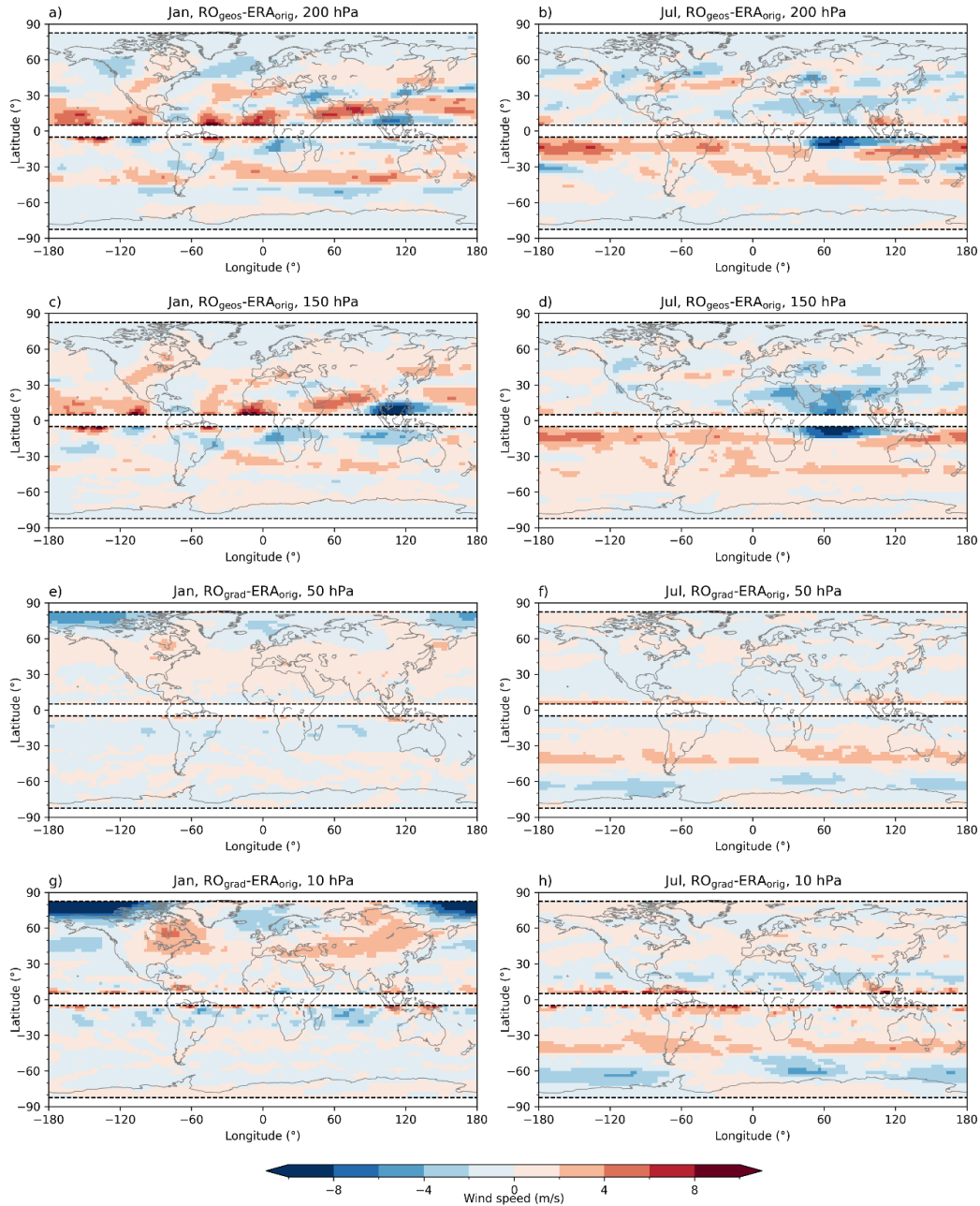
**Figure 10:** Long-term (2007–2020) mean total bias. Wind speed differences (m s$^{-1}$) between the geostrophic RO (RO$_{geos}$) and the original ERA5 (ERA$_{orig}$) wind, at 200 hPa (first row) and 150 hPa (second row) level, and between the gradient RO (RO$_{grad}$) and the original ERA5 (ERA$_{orig}$) wind, at 50 hPa (third row) and 10 hPa (last row) levels for January (left column) and July

(right column). Dashed black horizontal lines delineate the ±5° latitude band around the equator and ±82.5° regions toward poles.

## 4 Discussion

The main goal of this study was to test the general ability of RO-derived climatic winds to represent original ERA5 winds on the 2.5° × 2.5° horizontal grid. For this purpose, we decomposed the total wind speed bias into the contribution depending on the approximation method (approximation bias) and the contribution from the difference between the two datasets (systematic difference).

First, the ability of conventionally used local force balance approximations, geostrophic and gradient wind balance, to represent original monthly-mean wind speeds was evaluated based on the ERA5 reanalysis data. The validation was performed horizontally (from equator up to ±82.5° and from 180° W to 180° E) and vertically (from the bottom of the free troposphere at 800 hPa up to the middle stratosphere at 10 hPa). Testing commonly used methods to estimate wind speed based on the thermodynamic data, showed that regarding the limitations of the Coriolis parameter as one approaches equator, in the free troposphere it is possible to use approximations up to ±5° latitude. In the stratosphere it was possible to derive winds from the approximation towards ±2.5° latitude. However, since we focus on the long-term mean wind speed bias, an overestimation in the zonal/meridional wind component joint with a possible underestimation of the meridional/zonal component might result in a low total wind speed bias. This result is also supported by findings in Danzer et al. (2024). They comment that the break-down of the geostrophic balance is mainly related to a larger bias in the meridional component. This is why in the stratosphere, where tropical flow is dominantly zonal, the approximation bias is lower.

Even though the gradient wind approximation is a generalization of the geostrophic balance, it does not imply that it will always give the better estimation of the real wind. In accordance with earlier studies, the geostrophic approximation is a suitable method to describe a wind field in the free troposphere (Boville 1987; Scherllin-Prischer et al., 2014; Verkhoglyadova et al., 2014). We detected the dominant ageostrophic features in the area of the sub-tropical jet-stream and monsoonal region in the winter hemisphere, as well as above large mountain ranges in winter. The dipole patterns above mountains are related to the stationary waves which are quite common in the NH winter mid-latitudes. Still, due to long-term averaging, they are not as expressed as in Figure 2 in the study of Scherllin-Pirscher et al. (2014). Such features arise from the zonal differences in the topography, land-sea distribution and atmospheric diabatic heating. Their structure and magnitude depend on the characteristics of the jet-stream (Wills et al., 2019). Accordingly, long-term averaging might damp such features in regions where their inter-annual variability is larger. However, dipole structures related to the impact of Rocky Mountains and Himalaya on the large-scale wind flow (e.g., Sandu et al., 2019) are present in the long-term ageostrophic term. Hence, not

accounting for advection terms in the momentum equations fails to correctly reproduce these wave-mean flow interaction. On the other hand, thermally driven monsoonal circulation, shows small inter-annual variations in its direction and position, so its contribution to the ageostrophy is also well expressed in the long-term mean. Again, neglecting horizontal advection of momentum resulted in not well captured typical upper air monsoonal winds, with the strongest bias at around 150 hPa (Trenberth et al., 2000).

On the other hand, a larger contribution of curvature effects, as well as very strong winds, contribute to a better stratospheric wind field estimation (especially over the mid-latitudes) by using the gradient wind approximation (Elson 1986; Boville 1987; Randel 1987). Significant geostrophic wind overestimation in these regions is reduced by retaining the centrifugal term in the equations of motion. Even though the SH winter polar jet-stream is well described using the balanced gradient winds, this is not the case at the NH where the winter polar night jet-stream is more asymmetrical. Larger underestimation of the original wind by the gradient wind balance is detected in high-latitude regions at ~80°N, which was also found in other papers (Elson 1986; Randel 1987). This is due to the effect of the Aleutian high in those regions, a high-pressure system commonly found in the NH stratosphere during the winter season (Colucci and Ehrmann, 2018; Elson 1986; Harvey and Hitchman, 1996). By omitting horizontal advection terms (i.e., wave-flux terms), the effect of this pressure system on the jet-stream in this region is not well included resulting in the underestimation of the original wind by the gradient wind balance. Overall, both methods capture general features of global climatic winds on a synoptic scale, from the free troposphere to the mid-stratosphere, excluding the equatorial region.

The successful performance of the methods is of great importance for enabling a reliable long-term dynamical wind field monitoring based on the thermodynamic mass field data, such as available in the form of RO-derived isobaric geopotential height data. Hence, in a second step, we tested how well RO-derived climatic winds agree with the corresponding ones estimated from ERA5 reanalysis data. Here, we additionally test the temporal changes in this systematic difference to check for possible inhomogeneities. The analysis of the systematic differences between ERA5 and RO datasets revealed generally a good agreement over the whole near-global free troposphere-mid stratosphere domain. The largest differences are observed in the region of the sub-tropical jet-stream core. The systematic differences are larger in the lower levels compared to the upper ones. Even though the geopotential difference between the two data sets is quite small (here not shown), compared to the magnitude of the geopotential itself (below 1 %), we find that such small differences can lead to appreciable differences in wind speeds (up to 8 m s$^{-1}$), since these derive from the spatial derivatives of the isobaric geopotential fields.

A systematic underestimation in the centre of the sub-tropical jet-stream and an overestimation in its equator-ward parts indicates a difference in the sub-tropical jet-stream position between the two datasets. Mentioned deviations in the sub-tropical jet-stream is analysed in detail by testing its long-term stability using linear trend fits over 2007–2020. We estimated a trend magnitude of more than 0.5 m s$^{-1}$ per decade, which exceeds the WMO-GCOS (2016) long-term stability requirement. Besides temporal changes in the amplitude of the systematic difference, temporal differences in altitudinal direction are also observed.

Since RO-data are shown to be long-term stable (Steiner et al., 2020a), such findings might point to the effect of changes in the assimilated data in the ERA5 (Hersbach et al., 2020). This result indicates the potential advantage of RO-derived winds in terms of long-term stability for multi-decadal wind field monitoring, for example, to monitor the changes in large-scale circulation patterns such as the tropical-subtropical Hadley circulation (e.g., Weatherhead et al., 2018) or in the subtropical 500 and polar jet streams, respectively.

Generally, the approximation bias and the systematic difference are both larger in the winter hemisphere when the atmosphere is more dynamic in terms of larger wind speeds and stronger wave activity (Wu and Jehn 1972; Scherllin-Prischer et al., 2014, 2017; Verkhoglyadova et al., 2014). This is one of the reasons why early validation studies a few decades ago were mainly performed for the winter season, especially over the NH, as wave-activity is then more expressed (e.g., Elson 1986; Boville 505 1987; Randel 1987).

This study advances on earlier initial studies to derive wind fields based on RO data (Scherllin-Pirscher et al., 2014, 2017; Verkhoglyadova et al., 2014). One of the advances is the two-fold approach, where we decompose the total wind bias into a contribution from the wind approximation bias and another part coming from the systematic difference between the datasets. Scherllin-Prischer et al. (2014) commented that the total wind bias is mainly caused by the wind approximation used, compared 510 to the effect of RO retrieval errors. However, here we show that in the free troposphere region, the systematic difference between the two datasets in the sub-tropical jet-stream region is also contributing to the total bias. The finer horizontal grid used here (2.5°), compared to those of previous studies (5°), allowed us to go more equator-ward to reliably explore the region of the breakdown of the geostrophic approximation. While previous studies excluded the tropical regions between ±10° or ±15° (based on the argument of Coriolis force becoming small), we found that it is reliably possible to only exclude the ±5° 515 equatorial band in the free troposphere and ±2.5° band in the lower stratosphere. In addition, compared to the earlier studies, where few specific years were selected for the initial analyses, here we analysed long-term wind speed means, including the decadal-scale temporal stability, which gave more robust results.

## 5 Conclusions and perspectives

The investigation of the appropriate approximation method to derive winds, combined with the suitability of RO data to 520 estimate climatic winds based on the geopotential fields gave generally encouraging results.

Main findings include:

- Regarding the singularity of Coriolis parameter near the Equator, with the applied spatial grid of 2.5° latitude × 2.5° longitude, it is possible to use geostrophic/gradient wind approximations equatorward as close as down to 5° latitude in the free troposphere and 2.5° latitude in the lower stratosphere region,

525    – it is justified to use the geostrophic approximation as a method to estimate winds in the free troposphere, while for the stratospheric winds the additional inclusion of the centrifugal term contributes to better wind estimation,

    – in the free troposphere, larger ageostrophic contributions are found in the sub-tropical jet-stream region, over large mountain ranges and in the monsoon regions, due to neglecting the horizontal advection terms and/or vertical wind component in the equations of motion,

530    – in the stratosphere, the largest bias of the gradient wind approximation is detected in NH polar regions, where the effect of wave-jet-stream interaction is not included due to neglecting horizontal advection terms in the equations of motion,

    – the differences between RO and ERA5 geostrophic winds are generally small with values well within $\pm 2$ m s$^{-1}$, except in the region of the sub-tropical jet-stream, where patterns of latitudinal over- and underestimation are observed,

535    pointing to possible differences in the jet-stream position between the two datasets,

    – trend analysis of the detected jet-stream difference showed an exceeding of the WMO-GCOS (2016) 0.5 m s$^{-1}$ per decade stability requirement, pointing to an inhomogeneity in ERA5 data due to observing system changes and potential added-value from the long-term stability of RO-derived wind field records,

    – overall, the total difference between RO-derived wind (geostrophic wind in the free troposphere and gradient wind in

540    the stratosphere) and ERA5 original wind is small in monthly-mean wind fields, with differences in the troposphere due to both approximation bias and the systematic difference between the datasets and in the stratosphere due to the approximation bias.

Despite this decent progress towards assessing the utility of RO records for wind monitoring, some problems and questions remain. One of the future goals is to create a global climatic wind-speed dataset based on RO data. For these purposes the

545 equatorial region between $\pm 5°$ latitude, which was excluded here, needs to be filled. Healy et al. (2020) showed that RO-derived zonal mean balance winds well quantify stratospheric zonal winds at the equator. However, this equatorial-balance-approximation approach did not provide information on geographically gridded wind fields and appears to lack information towards lower altitudes into the free troposphere. Following Healy et al. (2020) and Scaife et al. (2000), Danzer et al. (2024) went a step further and derived wind fields in tropical region using the equatorial balance approximation. They also showed

550 that the geostrophic approximation works well in estimating zonal mean zonal wind in this region, while larger deviations are observed for the meridional wind component.

Hence, it is needed to combine these RO-estimated wind fields based on three different methods (equatorial wind balance in the tropics, geostrophic wind in the troposphere and gradient wind in the stratosphere) to derive physically meaningful wind field dataset. Additional improvements in approximation methods are needed in the regions where advection terms showed to

be important (e.g., NH winter mid-latitudes and monsoon region in free troposphere as well as stratospheric NH near-polar region). For these purposes, we plan to adapt and validate the methods proposed by Elson (1986) and Randel (1987).

Another avenue is the also-mentioned lower accuracy of RO data above about 30 km, mainly related to residual ionospheric biases. The potential of improving geopotential height data from RO at these altitudes does exist (e.g., Healy and Culverwell, 2015; Danzer et al., 2020, 2021; Liu et al., 2021; Syndergaard and Kirchengast, 2022), and the use of newest reprocessed RO data records is expected to also help improve wind monitoring in the upper stratosphere allowing wind estimation up to the 5 hPa level. With improved RO data accuracy, RO climatic winds might provide additional information about corresponding dynamics at these high altitudes. On the other hand, reanalysis assimilates less observational data towards higher altitudes (e.g., Podglajen et al., 2014), and the output is less observation-constrained and more strongly a result of the used model.

Overall, the added value of RO data is expected to be provided by its unique combination of fine vertical resolution, high accuracy and long-term stability over inter-annual to decadal time periods of climate change relevance. This capacity to accurately keep long-term consistency valuably complements the dense resolution and coverage qualities of reanalyses, where occasional inhomogeneities due to changes in observing systems are experienced. As stated in Hoffman et al. (2017): "*It is imperative that researchers understand the sources, uncertainty, biases and other limitations of any data that they use*".

For reanalyses that is not an easy task, due to the sources of uncertainties and errors arising from assimilated data, used numerical weather forecast model, and applied assimilation method (Parker 2016). In contrast, the uncertainties and errors in RO data are well understood and assessed (Steiner et al., 2020a). The potential for climate-related studies is manifold, and given the increasing observational database from the multi-satellite RO observing systems, RO climatic winds can serve as a valuable complementary data source for wind field monitoring and climate analyses.

**Author contribution**

Conceptualization: GK, JD; Data curation: IN; Formal analysis: IN, JD; Funding acquisition: JD; Investigation: IN, JD; Methodology: IN, JD, GK; Supervision: JD, GK; Validation & Visualisation: IN, JD, GK; Writing – original draft preparation: IN, JD; Writing – review & editing: IN, JD, GK.

**Acknowledgments**

We thank the UCAR/CDAAC RO team for providing RO excess phase and orbit data and the WEGC RO team for providing the OPSv5.6 retrieved profile data. We particularly thank F. Ladstädter (WEGC) for providing the monthly gridded RO climatology data and related discussions, M. Schwärz (WEGC) and H. Truhetz (WEGC) for providing ECMWF-IFS analysis data, and A. Reiter (WEGC) for proof-reading. Furthermore, we thank the ECMWF for providing access to the ERA5 reanalysis data. Finally, we thank the Austrian Science Fund (FWF) for funding the work; the wind analysis is part of the FWF stand-alone project Strato-Clim (grant number P-40182).

**Data Availability Statement**

The ERA5 data on pressure levels are retrieved directly on 2.5° × 2.5° resolution from ECMWF's Meteorological Archival

590 and Retrieval System (MARS). The OPSv5.6 data are available at the website (https://www.doi.org/10.25364/WEGC/OPS5.6:2020.1).

**Competing interests**

The authors have no competing interests.

## References

Angerer, B., Ladstädter, F., Scherllin-Pirscher, B., Schwärz, M., Steiner, A. K., Foelsche, U., and Kirchengast, G.: Quality aspects of the Wegener Center multi-satellite GPS radio occultation record OPSv5. 6, Atmos. Meas. Tech., 10(12), 4845–4863, https://doi.org/10.5194/amt-10-4845-2017, 2017.

Anthes, R. A.: Exploring Earth's atmosphere with radio occultation: Contributions to weather, climate and space weather, Atmos. Meas. Tech., 4(6), 1077, https://doi.org/10.5194/amt-4-1077-2011, 2011.

Anthes, R. A., Bernhardt, P. A., Chen, Y., Cucurull, L., Dymond, K. F., Ector, D., Healy, S. B., Ho, S.-P., Hunt, D. C., Kuo, Y. H., Liu, H., Manning, K., McCormick, C., Meehan, T. K., Randel, W. J., Rocken, C., Schreiner, W. S., Sokolovskiy, S. V., Syndergaard, S., Thompson, D. C., Trenberth, K. E., Wee, T. K., Yen, N. L., and Zeng, Z.: The COSMIC/FORMOSAT-3 mission: Early results, Bull. Amer. Meteor. Soc., 89, 313–333, https://doi.org/10.1175/BAMS-89-3-313, 2008.

Banyard, T. P., Wright, C. J., Hindley, N. P., Halloran, G., Krisch, I., Kaifler, B., and Hoffmann, L.: Atmospheric gravity waves in Aeolus wind lidar observations, Geophys. Res. Lett., 48, e2021GL092756, https://doi.org/10.1029/2021GL092756, 2021.

Basha, G., Kishore, P., Ratnam, M.V. *et al.* Global climatology of planetary boundary layer top obtained from multi-satellite GPS RO observations. *Clim Dyn* 52, 2385–2398. https://doi.org/10.1007/s00382-018-4269-1, 2019.

de la Beaujardière, O., Jeong, L., Basu, B., Basu, S., Beach, T., Bernhardt, P., Burke, W., Groves, K., Heelis, R., Holzworth, R., Huang, C., Hunton, D., Kelley, M., Pfaff, R., Retterer, J., Rich, F., Starks, M., Straus, P., and Valladares, C.: C/NOFS: a mission to forecast scintillations, J. Atmos. Sol. Terr. Phys., 1573–1591, https://doi.org/10.1016/j.jastp.2004.07.030, 2004.

Beyerle, G., Schmidt, T., Michalak, G., Heise, S., Wickert, J., and Reigber, C.: GPS radio occultation with GRACE: Atmospheric profiling utilizing the zero difference technique, Geophys. Res. Lett., 32, L13806, https://doi.org/10.1029/2005GL023109, 2005.

Boville, B. A.: The Validity of the Geostrophic Approximation in the Winter Stratosphere and Troposphere, J. Atmos. Sci., 44(2), 443–457, https://doi.org/10.1175/1520-0469(1987)044<0443:TVOTGA>2.0.CO;2, 1987.

Buontempo, C., Jupp, A. and Rennie, M.: Operational NWP assimilation of GPS radio occultation data, Atmos. Sci. Lett., 9: 129–133, https://doi.org/10.1002/asl.173, 2008.

Cardinali, C.: Monitoring the observation impact on the short-range forecast, Q. J. R. Meteorol. Soc., 135(638), 239–250, https://doi.org/10.1002/qj.366, 2009.

Colucci, S. J., and Ehrmann, T. S.: Synoptic–Dynamic Climatology of the Aleutian High. *J. Atmos. Sci.*, **75**, 1271–1283, https://doi.org/10.1175/JAS-D-17-0215.1., 2018

Danzer, J., Scherllin-Pirscher, B., and Foelsche, U.: Systematic residual ionospheric errors in radio occultation data and a potential way to minimize them, Atmos. Meas. Tech., 6, 2169–2179, https://doi.org/10.5194/amt-6-2169-2013, 2013.

Danzer, J., Schwärz, M., Proschek, V., Foelsche, U., and Gleisner, H.: Comparison study of COSMIC RO dry-air climatologies based on average profile inversion, Atmos. Meas. Tech., 11, 4867–4882, https://doi.org/10.5194/amt-11-4867-2018, 2018.

Danzer, J., Schwaerz, M., Kirchengast, G., and Healy, S. B.: Sensitivity analysis and impact of the kappa-correction of residual ionospheric biases on radio occultation climatologies, Earth Space Sci., 7, e2019EA000942, https://doi.org/10.1029/2019EA000942, 2020.

Danzer, J., Haas, S. J., Schwaerz, M., and Kirchengast, G.: Performance of the ionospheric kappa-correction of radio occultation profiles under diverse ionization and solar activity conditions, Earth Space Sci., 8, e2020EA001581, https://doi.org/10.1029/2020EA001581, 2021.

Danzer, J., Pieler, M., and Kirchengast, G.: Closing the gap in the tropics: the added value of radio-occultation data for wind field monitoring across the Equator, Atmos. Meas. Tech., 17, 4979–4995, https://doi.org/10.5194/amt-17-4979-2024, 2024.

Devaraju, B. Understanding Filtering on the Sphere—Experiences from Filtering GRACE Data. Ph.D. Thesis, Universität Stuttgart, Stuttgart, Germany, 2015.

Elson, L. S.: Ageostrophic Motions in the Stratosphere from Satellite Observations, J. Atmos. Sci., 43(5), 409-418, https://doi.org/10.1175/1520-0469(1986)043<0409:AMITSF>2.0.CO;2, 1986.

Eyre, J. R. , English, S. J., and Forsythe, M.:Assimilation of satellite data in numerical weather prediction. Part I: The early years, Q. J. R. Meteorol. Soc., 146, 49–68, https://doi.org/10.1002/qj.3654, 2020.

Foelsche, U., Scherllin-Pirscher, B., Ladstädter, F., Steiner, A. K., and Kirchengast, G.: Refractivity and temperature climate records from multiple radio occultation satellites consistent within 0.05%, Atmos. Meas. Tech., 4, 2007–2018, https://doi.org/10.5194/amt-4-2007-2011, 2011.

Gelaro, R., McCarty, W., Suárez, M. J., Todling, R., Molod, A., Takacs, L., Randles, C. A., Darmenov, A., Bosilovich, M. G., Reichle, R., Wargan, K., Coy, L., Cullather, R., Draper, C., Akella, S., Buchard, V., Conaty, A., da Silva, A. M., Gu, W., Kim, G., Koster, R., Lucchesi, R., Merkova, D., Nielsen, J. E., Partyka, G., Pawson, S., Putman, W., Rienecker, M., Schubert, S. D., Sienkiewicz, M., and Zhao, B.: The Modern-Era Retrospective Analysis for Research and Applications, Version 2 (MERRA-2), J. Clim., 30(14), 5419–5454, https://doi.org/10.1175/JCLI-D-16-0758.1, 2017.

Hajj, G. A., Ao, C. O., Iijima, B. A., Kuang, D., Kursinski, E. R., Mannucci, A. J., Meehan, T. K., Romans, L. J., de la Torre Juarez, M., and Yunck, T. P.: CHAMP and SAC-C atmospheric occultation results and intercomparisons. J. Geophys. Res. Atmos., 109, D06109. https://doi.org/10.1029/2003JD003909, 2004.

Harvey, V. L., and Hitchman, M. H.: A Climatology of the Aleutian High. *J. Atmos. Sci.*, **53**, 2088–2102, https://doi.org/10.1175/1520-0469(1996)053<2088:ACOTAH>2.0.CO;2, 1996

Healy, S. B., and Culverwell, I. D.: A modification to the standard ionospheric correction method used in GPS radio occultation, Atmos. Meas. Tech., 8(8), 3385–3393, https://doi.org/10.5194/amt-8-3385-2015, 2015.

Healy, S. B., and Thépaut J.-N.: Assimilation experiments with CHAMP GPS radio occultation measurements, Q. J. R. Meteorol. Soc., 132, 605–623, https://doi.org/10.1256/qj.04.182, 2006.

Healy, B, Polichtchouk, I., and Horányi, A.: Monthly and zonally averaged zonal wind information in the equatorial stratosphere provided by GNSS radio occultation, Q. J. R. Meteorol. Soc., 146: 3612– 3621, https://doi.org/10.1002/qj.3870, 2020.

Hersbach, H., Bell, B., Berrisford, P., Hirahara, S., Horányi, A., Muñoz-Sabater, J., ... and Thépaut, J. N.: The ERA5 global reanalysis, Q. J. R. Meteorol. Soc., 146(730), 1999–2049, https://doi.org/10.1002/qj.3803, 2020.

Hoffman, R. N., Privé, N., and Bourassa, M. Comments on "Reanalyses and observations: What's the difference?". Bulletin of the American Meteorological Society, 98(11), 2455-2459. https://doi.org/10.1175/BAMS-D-17-0008.1, 2017.

Holton, J. R., and Hakim, G. J. (2013). An introduction to dynamic meteorology (Vol. 88). Academic press.

Kanitz, T., Lochard, J., Marshall, J., McGoldrick, P., Lecrenier, O., Bravetti, P., Reitebuch, O., Rennie, M., Wernham, D., and Elfving, A.: Aeolus first light: first glimpse, in: International Conference on Space Optics—ICSO 2018, vol. 11180, pp. 659–664, SPIE, 2019.

Kawatani, Y., Hirooka, T., Hamilton, K., Smith, A. K., and Fujiwara, M.: Representation of the equatorial stratopause semiannual oscillation in global atmospheric reanalyses, Atmos. Chem. Phys., 20, 9115–9133, https://doi.org/10.5194/acp-20-9115-2020, 2020.

Kobayashi, S., Ota, Y., Harada, Y., Ebita, A., Moriya, M., Onoda, H., ... and Takahashi, K.: The JRA-55 reanalysis: General specifications and basic characteristics, J. Meteorol. Soc. Jpn. Ser. II, 93(1), 5–48, https://doi.org/10.2151/jmsj.2015-001, 2015.

Kursinski, E. R., Hajj, G. A., Schofield, J. T., Linfield, R. P., and Hardy, K. R.: Observing Earth's atmosphere with radio occultation measurements using the Global Positioning System, J. Geophys. Res. Atmos., 102(D19), 23429-23465, https://doi.org/10.1029/97JD01569, 1997.

Ladstädter, F.: Talk on gridding strategies, in: OPAC-IROWG 2022 conference, Seggau, Austria, Seggau Castle, 8–14 September 2022, https://static.uni-graz.at/fileadmin/veranstaltungen/opacirowg2022/programme/08.9.22/AM/Session_1/OPAC-IROWG-2022_Ladstaedter.pdf, (last access: 27 September 2024), 2022.

Li, Y., Kirchengast, G., Scherllin-Pirscher, B., Schwaerz, M., Nielsen, J. K., Ho, S. P., and Yuan, Y. B.: A new algorithm for the retrieval of atmospheric profiles from GNSS radio occultation data in moist air and comparison to 1DVar retrievals, Remote Sens., 11(23), 2729, https://doi.org/10.3390/rs11232729, 2019.

Liu, C., Kirchengast, G., Sun, Y., Zhang, K., Norman, R., Schwaerz, M., Bai, W., Du, Q., and Li, Y.: Analysis of ionospheric structure influences on residual ionospheric errors in GNSS radio occultation bending angles based on ray tracing simulations, Atmos. Meas. Tech., 11, 2427–2440, https://doi.org/10.5194/amt-11-2427-2018, 2018.

Liu, C., Kirchengast, G., Sun, Y., Proschek, V., Wang, X., Tian, L., Du, Q., Bai, W., Wu, C., Hu, P., and Tan G.:. Impacts of orbital and constellation parameters on the number and spatiotemporal coverage of LEO-LEO occultation events, Remote Sens., 13, 4849, https://doi.org/10.3390/rs13234849, 2021.

Luntama, J.-P., Kirchengast, G., Borsche, M., Foelsche, U., Steiner, A., Healy, S. B., von Engeln, A., O'Clerigh, E., and Marquardt, C.: Prospects of the EPS GRAS mission for operational atmospheric applications, Bull. Amer. Meteor. Soc., 89, 1863–1875, https://doi.org/10.1175/2008BAMS2399.1, 2008.

Mannucci, A.J., Ao, C.O., and Williamson, W.: GNSS Radio Occultation. In Position, Navigation, and Timing Technologies in the 21st Century (eds Y.T.J. Morton, F. Diggelen, J.J. Spilker, B.W. Parkinson, S. Lo and G. Gao), https://doi.org/10.1002/9781119458449.ch33, 2020.

Nimac, I., Danzer, J., and Kirchengast, G.: Validation of the geostrophic approximation using ERA5 and the potential of long-term radio occultation data for supporting wind field monitoring, Atmos. Meas. Tech. Discuss. [preprint], https://doi.org/10.5194/amt-2023-100, 2023.

Oberheide, J., Lehmacher, G. A., Offermann, D., Grossmann, K. U., Manson, A. H., Meek, C. E., Schmidlin, F. J., Singer, W., Hoffmann, P., and Vincent, R. A.: Geostrophic wind fields in the stratosphere and mesosphere from satellite data, J. Geophys. Res. Atmos., 107( D23), 8175, https://doi.org/10.1029/2001JD000655, 2002.

Parker, W. S. Reanalyses and observations: What's the difference?. Bulletin of the American Meteorological Society, 97(9), 1565-1572. https://doi.org/10.1175/BAMS-D-14-00226.1, 2016.

Podglajen, A., Hertzog, A., Plougonven, R., and Žagar, N.: Assessment of the accuracy of (re)analyses in the equatorial lower stratosphere, J. Geophys. Res. Atmos., 119, 11,166–11,188, https://doi.org/10.1002/2014JD021849, 2014.

Randel, W. J.: The evaluation of winds from geopotential height data in the stratosphere, J. Atmos. Sci., 44(20), 3097–3120, https://doi.org/10.1175/1520-0469(1987)044<3097:TEOWFG>2.0.CO;2, 1987.

Rennie, M.P., Isaksen, L., Weiler, F., de Kloe, J., Kanitz, T. and Reitebuch, O.: The impact of Aeolus wind retrievals on ECMWF global weather forecasts, Q. J. R. Meteorol. Soc., 147(740), 3555– 3586, https://doi.org/10.1002/qj.4142, 2021.

Rummukainen, M.: State-of-the-art with regional climate models, WIREs Clim Change, 1: 82–96, https://doi.org/10.1002/wcc.8, 2010.

Sandu, I., van Niekerk, A., Shepherd, T. G., Vosper, S. B., Zadra, A., Bacmeister, J., ... and Svensson, G.: Impacts of orography on large-scale atmospheric circulation. npj Climate and Atmospheric Science, 2(1), 10. https://doi.org/10.1038/s41612-019-0065-9, 2019.

Scaife, A. A., Austin, J., Butchart, N., Pawson, S., Keil, M., Nash, J., and James, I. N.: Seasonal and interannual variability of the stratosphere diagnosed from UKMO TOVS analyses, Quarterly Journal of the Royal Meteorological Society, 126, 2585–2604, https://doi.org/10.1002/qj.49712656812, 2000.

720 Scherllin-Pirscher, B., Steiner, A. K., Kirchengast, G., Kuo, Y.-H., and Foelsche, U.: Empirical analysis and modeling of errors of atmospheric profiles from GPS radio occultation, Atmos. Meas. Tech., 4, 1875–1890, https://doi.org/10.5194/amt-4-1875-2011, 2011a.

Scherllin-Pirscher, B., Kirchengast, G., Steiner, A. K., Kuo, Y.-H., and Foelsche, U.: Quantifying uncertainty in climatological fields from GPS radio occultation: an empirical-analytical error model, Atmos. Meas. Tech., 4, 2019–2034,
725 https://doi.org/10.5194/amt-4-2019-2011, 2011b.

Scherllin-Pirscher, B., Steiner, A. K., and Kirchengast, G.: Deriving dynamics from GPS radio occultation: Three-dimensional wind fields for monitoring the climate, Geophys. Res. Lett., 41, 7367–7374, https://doi.org/10.1002/2014GL061524, 2014.

Scherllin-Pirscher, B., Steiner, A. K., Kirchengast, G., Schwärz, M., and Leroy, S. S.: The power of vertical geolocation of atmospheric profiles from GNSS radio occultation, J. Geophys. Res. Atmos., 122, 1595–1616,
730 https://doi.org/10.1002/2016JD025902, 2017.

von Schuckmann, K., Minière, A., Gues, F., Cuesta-Valero, F. J., Kirchengast, G., Adusumilli, S., Straneo, F., Ablain, M., Allan, R. P., Barker, P. M., Beltrami, H., Blazquez, A., Boyer, T., Cheng, L., Church, J., Desbruyeres, D., Dolman, H., Domingues, C. M., García-García, A., Giglio, D., Gilson, J. E., Gorfer, M., Haimberger, L., Hakuba, M. Z., Hendricks, S., Hosoda, S., Johnson, G. C., Killick, R., King, B., Kolodziejczyk, N., Korosov, A., Krinner, G., Kuusela, M., Landerer, F. W.,
735 Langer, M., Lavergne, T., Lawrence, I., Li, Y., Lyman, J., Marti, F., Marzeion, B., Mayer, M., MacDougall, A. H., McDougall, T., Monselesan, D. P., Nitzbon, J., Otosaka, I., Peng, J., Purkey, S., Roemmich, D., Sato, K., Sato, K., Savita, A., Schweiger, A., Shepherd, A., Seneviratne, S. I., Simons, L., Slater, D. A., Slater, T., Steiner, A. K., Suga, T., Szekely, T., Thiery, W., Timmermans, M.-L., Vanderkelen, I., Wjiffels, S. E., Wu, T., and Zemp, M.: Heat stored in the Earth system 1960–2020: where does the energy go?, Earth Syst. Sci. Data, 15, 1675–1709, https://doi.org/10.5194/essd-15-1675-2023, 2023.

740 Steiner, A. K., Lackner, B. C., Ladstädter, F., Scherllin-Pirscher, B., Foelsche, U., and Kirchengast, G.; GPS radio occultation for climate monitoring and change detection, Radio Sci., 46, RS0D24, https://doi.org/10.1029/2010RS004614, 2011.

Steiner, A. K., Ladstädter, F., Ao, C. O., Gleisner, H., Ho, S.-P., Hunt, D., Schmidt, T., Foelsche, U., Kirchengast, G., Kuo, Y.-H., Lauritsen, K. B., Mannucci, A. J., Nielsen, J. K., Schreiner, W., Schwärz, M., Sokolovskiy, S., Syndergaard, S., and Wickert, J.: Consistency and structural uncertainty of multi-mission GPS radio occultation records, Atmos. Meas. Tech., 13,
745 2547–2575, https://doi.org/10.5194/amt-13-2547-2020, 2020a.

Steiner, A. K., Ladstädter, F., Randel, W. J., Maycock, A. C., Fu, Q., Claud, C., Gleisner, H., Haimberger, L., Ho, S.-P., Keckhut, P., Leblanc, T., Mears, C., Polvani, L. M., Santer, B. D., Schmidt, T., Sofieva, V., Wing, R., and Zou, C.-Z.: Observed Temperature Changes in the Troposphere and Stratosphere from 1979 to 2018, J. Clim., 33(19), 8165–8194, https://doi.org/10.1175/JCLI-D-19-0998.1, 2020b.

750 Stocker, M., Ladstädter, F., and Steiner, A. K.: Observing the climate impact of large wildfires on stratospheric temperature, Sci. Rep., 11(1), 1–11, https://doi.org/10.1038/s41598-021-02335-7, 2021.

Stoffelen, A., Pailleux, J., Källén, E., Vaughan, J. M., Isaksen, L., Flamant, P., Wergen, W., Andersson, E., Schyberg, H., Culoma, A., Meynart, R., Endemann, M., and Ingmann, P.: The atmospheric dynamics mission for global wind field measurement, Bull. Amer. Meteor. Soc., 86(1), 73–88, https://doi.org/10.1175/BAMS-86-1-73, 2005.

755 Stoffelen, A., Benedetti, A., Borde, R., Dabas, A., Flamant, P., Forsythe, M., Hardesty, M., Isaksen, L., Källén, E., Körnich, H., Lee, T., Reitebuch, O., Rennie, M., Riishøjgaard, L., Schyberg, H., Straume, A. G., and Vaughan, M.: Wind Profile Satellite Observation Requirements and Capabilities, Bull. Amer. Meteor. Soc., 101(11), E2005–E2021, https://doi.org/10.1175/BAMS-D-18-0202.1, 2020.

Syndergaard, S., and Kirchengast, G.: Systematic ionospheric residual errors in GNSS radio occultation: Theory for spherically 760 stratified media, Earth Space Sci., 9, e2022EA002335, https://doi.org/10.1029/2022EA002335, 2022.

Trenberth, K. E., Stepaniak, D. P. and Caron, J. M.: The Global Monsoon as Seen through the Divergent Atmospheric Circulation. J. Climate, **13**, 3969–3993, https://doi.org/10.1175/1520-0442(2000)013<3969:TGMAST>2.0.CO;2. 2000.

Verkhoglyadova, O. P., Leroy, S. S., and Ao, C. O.: Estimation of winds from GPS radio occultations, J. Atmos. Ocean. Technol., 31(11), 2451–2461, https://doi.org/10.1175/JTECH-D-14-00061.1, 2014.

765 Vishwakarma, B. D., Devaraju, B., Sneeuw, N.: What is the spatial resolution of GRACE satellite products for hydrology? Remote Sensing. 10(6):852. https://doi.org/10.3390/rs10060852, 2018.

Weatherhead, E.C., Wielicki, B.A., Ramaswamy, V., Abbott, M., Ackerman, T.P., Atlas, R., Brasseur, G., Bruhwiler, L., Busalacchi, A.J., Butler, J.H., Clack, C.T.M., Cooke, R., Cucurull, L., Davis, S.M., English, J.M., Fahey, D.W., Fine, S.S., Lazo, J.K., Liang, S., Loeb, N.G., Rignot, E., Soden, B., Stanitski, D., Stephens, G., Tapley, B.D., Thompson, A.M., Trenberth, 770 K.E. and Wuebbles, D.: Designing the climate observing system of the future, Earth's Future, 6: 80–102, https://doi.org/10.1002/2017EF000627, 2018.

Wickert, J., Reigber, C., Beyerle, G., König, R., Marquardt, C., Schmidt, T., Grunwaldt, L., Galas, R., Meehan, T. K., Melbourne, W. G., and Hocke, K.: Atmosphere sounding by GPS radio occultation: First results from CHAMP, Geophys. Res. Lett., 28(17), 3263–3266, https://doi.org/10.1029/2001GL013117, 2001.

775 Wickert, J., Beyerle, G., König, R., Heise, S., Grunwaldt, L., Michalak, G., Reigber, Ch., and Schmidt, T.: GPS radio occultation with CHAMP and GRACE: A first look at a new and promising satellite configuration for global atmospheric sounding, Ann. Geophys., 23, 653–658, https://doi.org/10.5194/angeo-23-653-2005, 2005.

Wills, R. C., White, R. H., and Levine, X. J. Northern Hemisphere stationary waves in a changing climate. Current climate change reports, 5, 372-389, https://doi.org/10.1007/s40641-019-00147-6, 2019.

780 Wu, H., and Jehn, K. H.: Geostrophic wind deviation in the upper troposphere and lower stratosphere in the El Paso–White Sands Area, Mon. Weather Rev., 100(2), 159–167, https://doi.org/10.1175/1520-0493(1972)100<0159:GWDITU>2.3.CO;2, 1972.

WMO-GCOS: The Global Observing System for Climate: Implementation Needs. GCOS-200. https://gcos.wmo.int/en/essential-climate-variables/about/requirements, last access: 05 December 2022, 2016.

785 WMO-OSCAR: Observing Systems Capability Analysis and Review Tool OSCAR Website https://space.oscar.wmo.int; re wind: https://space.oscar.wmo.int/variables/view/wind_horizontal, last access: 05 December 2022, 2022.

Zeng, Z., Sokolovskiy, S., Schreiner, W. S., and Hunt, D.: Representation of vertical atmospheric structures by radio occultation observations in the upper troposphere and lower stratosphere: Comparison to high-resolution radiosonde profiles, J. Atmos. Ocean. Technol., 36(4), 655–670, https://doi.org/10.1175/JTECH-D-18-0105.1, 2019.

790 Žagar, N., Rennie, M., and Isaksen, L.: Uncertainties in Kelvin waves in ECMWF analyses and forecasts: Insights from Aeolus observing system experiments, Geophys. Res. Lett., 48, e2021GL094716, https://doi.org/10.1029/2021GL094716, 2021.

## Appendix A
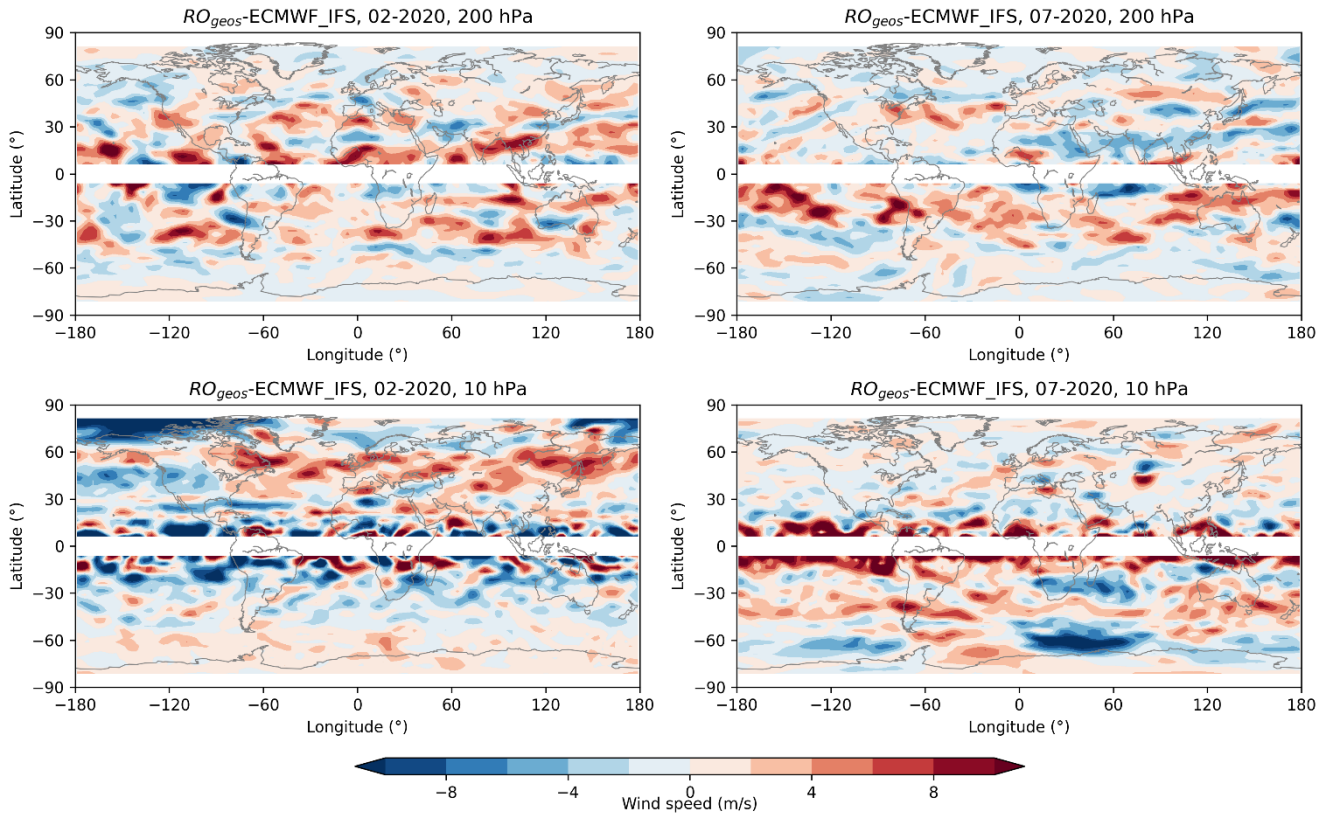
795

Figure A1. Difference between RO climatic and ECMWF-IFS wind speeds at 200 hPa level (top) and 10 hPa level (bottom), for February 2020 (left) and July 2020 (right), respectively.